Journal of
Mechanics of
Materials and Structures

A NEW MODELING APPROACH FOR PLANAR BEAMS: FINITE-ELEMENT SOLUTIONS BASED ON MIXED VARIATIONAL DERIVATIONS

Ferdinando Auricchio, Giuseppe Balduzzi and Carlo Lovadina

Volume 5, No. 5 May 2010

mathematical sciences publishers

JOURNAL OF MECHANICS OF MATERIALS AND STRUCTURES
Vol. 5, No. 5, 2010

A NEW MODELING APPROACH FOR PLANAR BEAMS: FINITE-ELEMENT SOLUTIONS BASED ON MIXED VARIATIONAL DERIVATIONS

FERDINANDO AURICCHIO, GIUSEPPE BALDUZZI AND CARLO LOVADINA

This paper illustrates a new modeling approach for planar linear elastic beams. Referring to existing models, we first introduce the variational principles that could be adopted for the beam model derivation, discussing their relative advantages and disadvantages. Then, starting from the Hellinger–Reissner functional we derive some homogeneous and multilayered beam models, discussing some properties of their analytical solutions. Finally, we develop a planar beam finite element, following an innovative approach that could be seen as the imposition of equilibrium in the cross-section and compatibility along the axis. The homogeneous model is capable of reproducing the behavior of the Timoshenko beam, with the advantage that the shear correction factor appears naturally from the variational derivation; the multilayered beam is capable of capturing the local effects produced by boundary constraints and load distributions; the finite element is capable of predicting the cross-section stress distribution with high accuracy, and more generally the behavior of planar structural elements.

1. Introduction

To reproduce the mechanical behavior of structural elements characterized by having one dimension predominant with respect to the other two (that is, a beam) the classical approaches are the well-known Euler–Bernoulli (EB) and Timoshenko theories [Timoshenko 1955; Hjelmstad 2005]. Generally adopted for very slender elements, the EB beam model assumes the cross-section axial and transverse displacements as 1D unknown fields, converting the 3D elastic problem, formulated through a set of partial differential equations, into a simpler system of two ordinary differential equations (ODEs). On the other hand, the Timoshenko beam model, adopted for less slender structural elements, assumes the cross-section axial and transverse displacements, together with rotations, as 1D fields, leading to a set of three ODEs. As a consequence of the field assumptions, these models are often referred to in the literature as *first-order* models. Moreover, we denote these models as *displacement-based* to underline that usually these models consider only the displacements as independent variables and the stresses are evaluated by postprocessing.

Despite their simplicity (also related to the possibility of computing analytical solutions) and their excellent first-design ability, the EB and Timoshenko models have some well-known limitations:

- loss of accuracy for beams with a low ratio between the length and cross-sectional characteristic dimension,

Keywords: laminated linear elastic beam, analytical solution, finite element modeling, mixed variational formulation.
The authors would like to thank professors Elio Sacco, Alessandro Reali, and Giancarlo Sangalli for several helpful suggestions during the completion of this work.

- loss of accuracy in modeling nonhomogeneous beams (such as composites) as well as in modeling nonlinear material behavior, and
- difficulty in computing accurate stress profiles, connected to the fact that only mean-value displacements are assumed as field variables.

Hence, due to the need for more accurate 1D models, researchers have developed new approaches that can generally be classified as

- *higher-order displacement-based models*, which introduce more sophisticated cross-section kinematics, and
- *mixed or hybrid models*, which also introduce stresses — and sometimes even strains — as independent variables.

To give a few examples, an often cited model falling in the first category is the one proposed in [Reddy 1984] that introduces section warping in addition to Timoshenko displacements. As discussed in [Sheinman 2001], this model shows inconsistencies, since transverse displacement generates a constant cross-section shear distribution, whereas axial displacements yield a quadratic one. More complete kinematics are adopted in the model proposed by Lo et al. [1977a] where, considering both section warping and striction, authors eliminate such inconsistencies. For a general treatment of higher-order, planar, kinematic beam models and discussion of their analytical solutions readers may refer to the work of Sheinman [2001].

With respect to mixed models, a very interesting approach is the one proposed by Alessandrini et al. [1999], where, starting from 3D elasticity, the authors illustrate a clear derivation of some plate models, and also study the convergence of the models under consideration.

In terms of numerical modeling, the number of finite element (FE) implementations proposed in the literature is truly vast, since many different choices are possible, depending on

- *functional formulation and independent variables:* the simplest functionals consider only kinematic variables, as in displacement based beam models, while the most complicated also consider stresses and strains;
- *order of field approximation:* in addition to the first- versus higher-order classification, for the case of multilayered beams, *layerwise* models adopt piecewise layer-defined functions while *global* models use globally defined functions to describe the field distribution on a cross-section.

For both items, intermediate choices are possible, for example, only some stress components could be selected as independent variables, or some fields described layerwise, with the remaining ones assumed as global functions.

We note that in the available review papers (for example, [Carrera 2000; Wanji and Zhen 2008]), models are usually compared by considering different field approximations derived from the same principle. Therefore, it is possible to understand the effect of basis accuracy, but not improvements arising from the use of a more sophisticated variational principle. In Section 3 of this paper we review different variational principles that can be employed, briefly discussing their features and possible drawbacks.

The main aim of this paper is to propose a simple analytical model and an FE capable of capturing the section stress distribution with high accuracy as well as in a multilayered body. We opt for the *dimension reduction variational* approach, classical in beam modeling and used in Alessandrini et al. [1999] and

elsewhere for plate problems. This method might allow us to generalize the model to more complex situations, such as nonlinear constitutive laws.

A summary of the paper is as follows. In Section 2 we define the problem we are going to tackle. In Section 3 we introduce the functionals which may be used for the model derivation, listing for each one properties and developed models presented in the literature; by means of this discussion we are able to choose an appropriate variational principle as the starting point for the model derivations. In Section 4 we derive some 1D models. In Section 5 we present a few examples, giving some insight on the structure of the corresponding analytical solution. In Section 6 we develop suitable FE schemes, and present some results to illustrate their actual computational performances.

2. Problem definition

The object of our study is a planar beam Ω, not necessarily homogeneous along the thickness and modeled as a 2D body; this is equivalent to imposing the plane stress state hypotheses to a 3D body or to stating that the beam width is negligible. Moreover, we limit the discussion to linear elastic isotropic materials and small displacements.

We define the problem domain as: $\Omega = l \times A$, where the beam longitudinal axis l and the cross-section A are defined as:

$$l = \{x \in \mathbb{R} \mid x \in [0, \bar{l}]\}, \qquad A = \left\{ y \in \mathbb{R} \,\middle|\, y \in \left[-\frac{h}{2}, \frac{h}{2}\right] \right\},$$

in which h is the beam thickness and $\bar{l}$ is the beam length.

Obviously $\bar{l} \gg h$, so the longitudinal axis is the predominant dimension of the body. Figure 1 represents the domain and the adopted Cartesian coordinate system.

As illustrated in Figure 1 we define the lower and upper boundaries as S_0 and S_n, respectively, and the lateral cross-sections as A_0 and A_l. We denote the domain boundary as $\partial\Omega$, so that

$$\partial\Omega = (A_0 \cup A_l) \cup (S_0 \cup S_n).$$

For $\partial\Omega$, we consider the partition $\{\partial\Omega_t; \partial\Omega_s\}$, where $\partial\Omega_t$ and $\partial\Omega_s$ are the externally loaded and displacement constrained boundaries, respectively. The external load is defined as a line force density $\boldsymbol{t} : \partial\Omega_t \to \mathbb{R}^2$ while the body load is defined as an area force density $\boldsymbol{f} : \Omega \to \mathbb{R}^2$; we specify a sufficiently smooth boundary displacement function $\bar{\boldsymbol{s}} : \partial\Omega_s \to \mathbb{R}^2$. Finally, we suppose that the beam is made of layers whose thickness is constant along the axial coordinate x, though not necessarily the same at each layer. Consequently, the Young's modulus E and the Poisson's ratio ν are scalar fields depending on the thickness coordinate y, that is, $E : A \to \mathbb{R}$ and $\nu : A \to \mathbb{R}$.

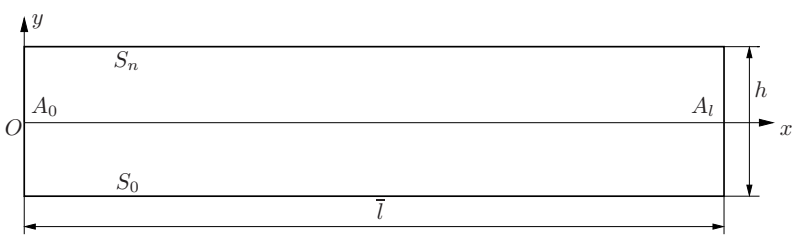

Figure 1. Planar beam geometry, coordinate system, dimensions, and adopted notations.

Introducing the independent variable fields $\boldsymbol{\sigma} : \Omega \to \mathbb{R}^{2\times 2}$, $\boldsymbol{\varepsilon} : \Omega \to \mathbb{R}^{2\times 2}$, and $\boldsymbol{s} : \Omega \to \mathbb{R}^2$, where the stress $\boldsymbol{\sigma}$ and the strain $\boldsymbol{\varepsilon}$ are symmetric tensors while the displacement $\boldsymbol{s}$ is a vector, the strong formulation of the problem under investigation corresponds to the following boundary value problem:

$$\boldsymbol{\varepsilon} = \nabla^s \boldsymbol{s}, \quad \boldsymbol{\sigma} = \boldsymbol{D} : \boldsymbol{\varepsilon}, \quad \nabla \cdot \boldsymbol{\sigma} + \boldsymbol{f} = \boldsymbol{0} \quad \text{in } \Omega; \qquad \boldsymbol{\sigma} \cdot \boldsymbol{n} = \boldsymbol{t} \quad \text{on } \partial\Omega_t; \qquad \boldsymbol{s} = \bar{\boldsymbol{s}} \quad \text{on } \partial\Omega_s. \tag{1}$$

Here $\boldsymbol{\varepsilon} = \nabla^s \boldsymbol{s}$ is the compatibility relation, $\boldsymbol{\sigma} = \boldsymbol{D} : \boldsymbol{\varepsilon}$ is the material constitutive relation, in which $\boldsymbol{D}$ is the appropriate fourth-order linear elastic tensor, and $\nabla \cdot \boldsymbol{\sigma} + \boldsymbol{f} = \boldsymbol{0}$ represents the equilibrium condition. The last two equations in (1) represent the boundary equilibrium and the boundary compatibility condition.

3. Variational problem formulations and modeling methods

In this section we are going to present different possible variational formulations for problem (1). In particular, we introduce approaches based on total potential energy and Hellinger–Reissner and Hu–Washizu functionals, considering for each different possible stationarity conditions. Restricting ourselves to the framework of Section 2, we emphasize that a variational beam model can be considered as the outcome of the following general procedure:

- **Step 1:** A variational principle is selected for the 2D planar elasticity problem. In particular, the functional spaces for the involved fields has to be appropriately chosen.
- **Step 2:** For each field involved, an approximation profile is selected. Typically, to develop a beam model, one chooses polynomial or piecewise polynomial shapes along the thickness direction, while no profile restrictions are imposed along the axial direction. However, the approximation fields should fit the functional framework of Step 1, at least if a *conforming* model is considered.
- **Step 3:** Integration along the thickness direction is performed. This way, the 2D variational problem is reduced to a 1D variational problem, which corresponds to a system of ODEs equipped with boundary conditions (that is, the beam model).

3.1. ***Total potential energy approach.*** Total potential energy (TPE) is the functional most frequently used in continuum mechanics and in the standard literature (for example, [Hjelmstad 2005]); several authors use it as a starting point to derive first-order beam models and the most popular corresponding FE formulations. The TPE functional can be expressed as follows:

$$J_{\mathrm{TPE}}(\boldsymbol{s}) = \frac{1}{2}\int_\Omega \nabla^s \boldsymbol{s} : \boldsymbol{D} : \nabla^s \boldsymbol{s}\, d\Omega - \int_\Omega \boldsymbol{s} \cdot \boldsymbol{f}\, d\Omega. \tag{2}$$

Boundary conditions will be suitably imposed as follows. The critical point of the functional above corresponds to finding the energy minimizer, which is unique and stable in the usual framework of admissible displacement space.

Requiring stationarity of the TPE (2), we obtain the following weak problem: *Find* $\boldsymbol{s} \in W^s$ *such that, for all* $\delta\boldsymbol{s} \in \overline{W}^s$,

$$\delta J^s_{\mathrm{TPE}} = \int_\Omega \nabla^s(\delta\boldsymbol{s}) : \boldsymbol{D} : \nabla^s \boldsymbol{s}\, d\Omega - \int_\Omega \delta\boldsymbol{s} \cdot \boldsymbol{f}\, d\Omega - \int_{\partial\Omega_t} \delta\boldsymbol{s} \cdot \boldsymbol{t}\, dS = 0, \tag{3}$$

where $W^s := \{\boldsymbol{s} \in H^1(\Omega) : \boldsymbol{s}|_{\partial\Omega_s} = \bar{\boldsymbol{s}}\}$ and $\overline{W}^s := \{\delta\boldsymbol{s} \in H^1(\Omega) : \delta\boldsymbol{s}|_{\partial\Omega_s} = \boldsymbol{0}\}$.

Equation (3) is called *symmetric TPE stationarity*. It is often used as a basis for FE development, leading obviously to a symmetric stiffness matrix.

Wanji and Zhen [2008] give a review of multilayered, elastic, displacement-based (that is, TPE derived) plate FE. Increasing orders of field approximation are considered, from the simplest models, in which displacements are globally defined along the cross-section, to the most sophisticated, in which displacements are defined layerwise. In the same reference it is noted that almost all the FEs presented perform only for specific problems, such as thick laminated plates or soft-core sandwiches; they are not able to accurately describe the shear distribution along the thickness in the general case.

An accurate evaluation of shear distribution is one of the aims of [Vinayak et al. 1996a; 1996b], in which the authors develop a multilayered planar beam FE starting from (3), using the field approximation proposed in [Lo et al. 1977a; 1977b] and appropriately treating the thickness heterogeneity. They propose two ways to evaluate the axial and transverse stresses: the first uses the compatibility and the constitutive relations $(1)_{1,2}$, while the second refines the shear and out-of-plane stress distributions using the equilibrium relation $(1)_3$. The resulting numerical schemes are generally satisfactory, but the computed solutions might exhibit instabilities near the boundary, and the stress distributions are not always sufficiently accurate.

As a general remark [Rohwer and Rolfes 1998; Rohwer et al. 2005], in TPE-based models the critical step is the postprocessing stress evaluation which could compromise the effectiveness of the method.

3.2. ***Hellinger–Reissner approach.*** The Hellinger–Reissner (HR) functional can be expressed as

$$J_{\mathrm{HR}}(\boldsymbol{\sigma}, \boldsymbol{s}) = \int_\Omega \boldsymbol{\sigma} : \nabla^s \boldsymbol{s}\, d\Omega - \frac{1}{2}\int_\Omega \boldsymbol{\sigma} : \boldsymbol{D}^{-1} : \boldsymbol{\sigma}\, d\Omega - \int_\Omega \boldsymbol{s}\cdot\boldsymbol{f}\, d\Omega. \tag{4}$$

How boundary conditions are enforced depends on the specific variational formulation employed to express the stationarity of the functional (see Sections 3.2.1 and 3.2.2). We also wish to remark that stationarity of this functional corresponds to a saddle point problem. Therefore, the model derivation based on the HR functional requires particular care in the displacement and stress field assumptions, otherwise the model risks leading to a problem which is not well-posed.

3.2.1. *HR grad-grad stationarity.* Requiring stationarity of the HR functional (4), we obtain the following weak problem: *Find* $\boldsymbol{s} \in W_{\bar{\boldsymbol{s}}}^{\mathrm{gg}}$ *and* $\boldsymbol{\sigma} \in S^{\mathrm{gg}}$ *such that, for all* $\delta\boldsymbol{s} \in \overline{W}^{\mathrm{gg}}$ *and all* $\delta\boldsymbol{\sigma} \in S^{\mathrm{gg}}$,

$$\delta J_{\mathrm{HR}}^{\mathrm{gg}} = \int_\Omega \nabla^s \delta\boldsymbol{s} : \boldsymbol{\sigma}\, d\Omega + \int_\Omega \delta\boldsymbol{\sigma} : \nabla^s \boldsymbol{s}\, d\Omega - \int_\Omega \delta\boldsymbol{\sigma} : \boldsymbol{D}^{-1} : \boldsymbol{\sigma}\, d\Omega - \int_\Omega \delta\boldsymbol{s}\cdot\boldsymbol{f}\, d\Omega - \int_{\partial\Omega_t} \delta\boldsymbol{s}\cdot\boldsymbol{t}\, dS = 0, \tag{5}$$

where $W_{\bar{\boldsymbol{s}}}^{\mathrm{gg}} := \{\boldsymbol{s} \in H^1(\Omega) : \boldsymbol{s}|_{\partial\Omega_s} = \bar{\boldsymbol{s}}\}$, $\overline{W}^{\mathrm{gg}} := \{\delta\boldsymbol{s} \in H^1(\Omega) : \delta\boldsymbol{s}|_{\partial\Omega_s} = \boldsymbol{0}\}$, and $S^{\mathrm{gg}} := \{\boldsymbol{\sigma} \in L^2(\Omega)\}$.

Equation (5) is called *HR grad-grad stationarity* because two gradient operators appear in the formulation. We remark that the kinematic boundary condition $\boldsymbol{s}|_{\partial\Omega_s} = \bar{\boldsymbol{s}}$ is directly enforced in the trial space $W_{\bar{\boldsymbol{s}}}^{\mathrm{gg}}$ (an *essential* boundary condition), while $\boldsymbol{\sigma}\cdot\boldsymbol{n}|_{\partial\Omega_t} = \boldsymbol{t}$ turns out to be a *natural* boundary condition.

As mentioned in Section 1, Alessandrini et al. [1999] derived some homogeneous plate models starting from HR grad-grad stationarity (5). They noticed that in many situations, models derived from (5) lead to displacement fields that minimize the potential energy in the class of the same kinematic assumptions. Therefore, in those cases HR grad-grad models are essentially equivalent to the corresponding models obtained by symmetric TPE stationarity (3).

Many researchers have derived multilayered plate and beam FEs using HR grad-grad stationarity. [Spilker 1982; Feng and Hoa 1998; Huang et al. 2002; Icardi and Atzori 2004] are among the most significant examples, since the computed solutions are generally satisfactory. The main drawback of these schemes, especially for the case of layerwise beams and plates, is the high number of degrees of freedom (DOFs), which leads to a heavy FE formulation. Spilker [1982] alleviates this problem by assuming the stress variables to be discontinuous along the plate extension so that they can be condensed at the element level reducing the mixed local stiffness matrix to a displacement-like one. An alternative is to consider some stress components as dependent variables, expressing them a priori in terms of the displacements. Reissner's mixed variational theorem [1986] follows this approach: the out of plane stresses τ_{xy} and σ_{yy} are considered as independent variables while the axial stress σ_{xx} is expressed as a function of displacements. In [Carrera 2000; 2001; Carrera and Demasi 2002; Demasi 2009a; 2009b; 2009c; 2009d; 2009e] various plate FEs are derived applying this viewpoint, with different choices of basis function, obtaining reasonable accuracy in the stress description. Unfortunately these authors are forced to use a high number of kinematic DOFs, drastically increasing the computational effort.

3.2.2. *HR div-div stationarity.* Integrating by parts, the first and the second terms of (5) become:

$$\int_\Omega \nabla^s \delta\boldsymbol{s} : \boldsymbol{\sigma}\, d\Omega = \int_{\partial\Omega} \delta\boldsymbol{s}\cdot\boldsymbol{\sigma}\cdot\boldsymbol{n}\, dS - \int_\Omega \delta\boldsymbol{s}\cdot\nabla\cdot\boldsymbol{\sigma}\, d\Omega, \quad \int_\Omega \delta\boldsymbol{\sigma} : \nabla^s \boldsymbol{s}\, d\Omega = \int_{\partial\Omega} \delta\boldsymbol{\sigma}\cdot\boldsymbol{n}\cdot\boldsymbol{s}\, dS - \int_\Omega \nabla\cdot\delta\boldsymbol{\sigma}\cdot\boldsymbol{s}\, d\Omega. \quad (6)$$

Hence, substituting (6) into (5), the weak formulation becomes: *Find* $\boldsymbol{s} \in W^{\mathrm{dd}}$ *and* $\boldsymbol{\sigma} \in S_t^{\mathrm{dd}}$ *such that, for all* $\delta\boldsymbol{s} \in W^{\mathrm{dd}}$ *and all* $\delta\boldsymbol{\sigma} \in \bar{S}^{\mathrm{dd}}$,

$$\delta J_{\mathrm{HR}}^{\mathrm{dd}} = -\int_\Omega \delta\boldsymbol{s}\cdot\nabla\cdot\boldsymbol{\sigma}\, d\Omega - \int_\Omega \nabla\cdot\delta\boldsymbol{\sigma}\cdot\boldsymbol{s}\, d\Omega - \int_\Omega \delta\boldsymbol{\sigma} : \boldsymbol{D}^{-1} : \boldsymbol{\sigma}\, d\Omega - \int_\Omega \delta\boldsymbol{s}\cdot\boldsymbol{f}\, d\Omega + \int_{\partial\Omega_s} \delta\boldsymbol{\sigma}\cdot\boldsymbol{n}\cdot\bar{\boldsymbol{s}}\, dS = 0, \quad (7)$$

where $W^{\mathrm{dd}} := \{\boldsymbol{s} \in L^2(\Omega)\}$, $S_t^{\mathrm{dd}} := \{\boldsymbol{\sigma} \in H(\mathrm{div}, \Omega) : \boldsymbol{\sigma}\cdot\boldsymbol{n}|_{\partial\Omega_t} = \boldsymbol{t}\}$, $\bar{S}^{\mathrm{dd}} := \{\delta\boldsymbol{\sigma} \in H(\mathrm{div}, \Omega) : \delta\boldsymbol{\sigma}\cdot\boldsymbol{n}|_{\partial\Omega_t} = \boldsymbol{0}\}$. Here and in what follows, $H(\mathrm{div}, \Omega)$ denotes the space of square-integrable vector functions whose divergence is still square-integrable.

Equation (7) is called *HR div-div stationarity* because two divergence operators appear in it. We remark that $\boldsymbol{s}|_{\partial\Omega_s} = \bar{\boldsymbol{s}}$ is now a *natural* boundary condition, while $\boldsymbol{\sigma}\cdot\boldsymbol{n}|_{\partial\Omega_t} = \boldsymbol{t}$ becomes an *essential* boundary condition, as it is directly incorporated in the space S_t^{dd}.

Considering the HR div-div stationarity approach (7), Alessandrini et al. [1999] have derived some homogeneous plate models, which are more interesting than the ones stemming from the HR grad-grad stationarity (5). However, the techniques developed in that work cannot be directly applied to general heterogeneous plates, because the resulting models may be divergent; see [Auricchio et al. 2004].

3.3. ***Hu–Washizu approach.*** The Hu–Washizu (HW) functional may be expressed as

$$J_{\mathrm{HW}}(\boldsymbol{\sigma}, \boldsymbol{\varepsilon}, \boldsymbol{s}) = \int_\Omega \boldsymbol{\sigma} : (\nabla^s \boldsymbol{s} - \boldsymbol{\varepsilon})\, d\Omega + \frac{1}{2}\int_\Omega \boldsymbol{\varepsilon} : \boldsymbol{D} : \boldsymbol{\varepsilon}\, d\Omega - \int_\Omega \boldsymbol{s}\cdot\boldsymbol{f}\, d\Omega. \quad (8)$$

Again, how boundary conditions are enforced depends on the specific variational formulation employed to express the stationarity of the functional. Here also the strain field is a primal variable. In the following variational formulations, we will not specify the functional frameworks for the involved fields, since they are similar to the ones of the HR-based corresponding variational formulations.

3.3.1. *HW grad-grad stationarity.* Stationarity of (8) can be expressed as

$$\delta J_{\mathrm{HW}}^{\mathrm{gg}} = \int_\Omega \nabla^s \delta \boldsymbol{s} : \boldsymbol{\sigma}\, d\Omega - \int_\Omega \delta\boldsymbol{\varepsilon} : \boldsymbol{\sigma}\, d\Omega + \int_\Omega \delta\boldsymbol{\sigma} : (\nabla^s \boldsymbol{s} - \boldsymbol{\varepsilon})\, d\Omega + \int_\Omega \delta\boldsymbol{\varepsilon} : \boldsymbol{D} : \boldsymbol{\varepsilon}\, d\Omega - \int_\Omega \delta\boldsymbol{s}\cdot\boldsymbol{f}\, d\Omega - \int_{\partial\Omega_t} \delta\boldsymbol{s}\cdot\boldsymbol{t}\, dS = 0, \quad (9)$$

where $\boldsymbol{s}$ satisfies $\boldsymbol{s}|_{\partial\Omega_s} = \bar{\boldsymbol{s}}$, while $\boldsymbol{\sigma}\cdot\boldsymbol{n}|_{\partial\Omega_t} = \boldsymbol{t}$ is a natural boundary condition. Equation (9) is called *HW grad-grad stationarity*; an example of its use in multilayered plate modeling is presented in [Auricchio and Sacco 1999].

3.3.2. *HW div-div stationarity.* A second formulation of HW stationarity can be found by introducing (6) into (9), obtaining

$$\delta J_{\mathrm{HW}}^{\mathrm{dd}} = -\int_\Omega \delta\boldsymbol{s}\cdot\nabla\cdot\boldsymbol{\sigma}\, d\Omega - \int_\Omega \delta\boldsymbol{\varepsilon} : \boldsymbol{\sigma}\, d\Omega - \int_\Omega \nabla\cdot\delta\boldsymbol{\sigma}\cdot\boldsymbol{s}\, d\Omega - \int_\Omega \delta\boldsymbol{\sigma} : \boldsymbol{\varepsilon}\, d\Omega + \int_\Omega \delta\boldsymbol{\varepsilon} : \boldsymbol{D} : \boldsymbol{\varepsilon}\, d\Omega - \int_\Omega \delta\boldsymbol{s}\cdot\boldsymbol{f}\, d\Omega + \int_{\partial\Omega_s} (\delta\boldsymbol{\sigma}\cdot\boldsymbol{n})\cdot\bar{\boldsymbol{s}}\, dS = 0, \quad (10)$$

where $\boldsymbol{\sigma}$ satisfies $\boldsymbol{\sigma}\cdot\boldsymbol{n} = \boldsymbol{t}$ on $\partial\Omega_t$, while $\boldsymbol{s}|_{\partial\Omega_s} = \bar{\boldsymbol{s}}$ is a natural boundary condition. This is called *HW div-div stationarity*.

3.4. ***Conclusions on weak formulations.*** We summarize the previous discussion in a few observations (see also Table 1):

- All the weak formulations considered are symmetric.
- Each mixed weak formulation can be expressed in different formats: the grad-grad formulations (5) and (9) and the div-div formulations (7) and (10). The former require considering a priori smooth displacement fields and less regular stress fields ($\boldsymbol{s} \in H^1(\Omega)$ and $\boldsymbol{\sigma} \in L^2(\Omega)$), while the latter demand a priori less regular displacement fields and smooth stress fields ($\boldsymbol{s} \in L^2(\Omega)$ and $\boldsymbol{\sigma} \in H(\mathrm{div}, \Omega)$).
- When selecting the approximation fields for the mixed model design (see Step 2 of the procedure described at the beginning of this section), the combination of the regularity requirements and the well-posedness of the corresponding saddle point problems typically leads to congruent models for the grad-grad formulations and self-equilibrated models for the div-div formulations.

In our view, one of the major limitations of the available elementary beam models is that equilibrium equations are not sufficiently enforced within the cross-section. For this reason we will focus on HR formulations, with some emphasis on the div-div form (7).

	Principle		
Displacement-based	TPE	Equation (3)	
Mixed	HR HW	grad-grad (5) grad-grad (9)	div-div (7) div-div (10)

Table 1. Functional stationarities classified in terms of the functionals from which they are derived and equation formats.

4. Model derivations

In this section we develop some beam models. We will start from the HR variational formulations of Section 3.2 (this is Step 1 of the procedure described at the beginning of Section 3), then define the approximated fields (Step 2), and perform the integration along the thickness (Step 3). To simplify further discussion, we will switch to engineering notation, the equivalence between tensor and engineering notation being summarized as follows, where $\boldsymbol{E}_1 = \left[\begin{smallmatrix}1&0&0\\0&0&1\end{smallmatrix}\right]$ and $\boldsymbol{E}_2 = \left[\begin{smallmatrix}0&0&0\\0&1&1\end{smallmatrix}\right]$:

Tensor notation	Engineering notation
$\nabla \cdot \boldsymbol{\sigma}$	$\left(\frac{d}{dx}\boldsymbol{E}_1 + \frac{d}{dy}\boldsymbol{E}_2\right)\boldsymbol{P}_\sigma \hat{\boldsymbol{\sigma}}$
$\nabla^S \boldsymbol{s}$	$\left(\frac{d}{dx}\boldsymbol{E}_1^T + \frac{d}{dy}\boldsymbol{E}_2^T\right)\boldsymbol{P}_s \hat{\boldsymbol{s}}$
$\boldsymbol{\sigma} \cdot \boldsymbol{n}$	$(n_x \boldsymbol{E}_1 + n_y \boldsymbol{E}_2)\boldsymbol{P}_\sigma \hat{\boldsymbol{\sigma}}$

4.1. ***Profile approximation and notations.*** We now introduce the notation we use for a generic approximated field $\gamma(x, y)$ involved in the beam models. We first define a *profile* vector function $\boldsymbol{p}_\gamma(y)$: $\boldsymbol{p}_\gamma : A \to \mathbb{R}^m$. We insist that the m components of $\boldsymbol{p}_\gamma(y)$ are a set of *linearly independent* functions of the cross-section coordinate y. They may be global polynomials, as well as piece-wise polynomials or other shape functions. The approximate field $\gamma(x, y)$ is expressed as a linear combination of the components of $\boldsymbol{p}_\gamma(y)$, with arbitrary functions of the axial coordinate x as coefficients, collected in a vector $\hat{\boldsymbol{\gamma}}(x)$. Therefore, $\gamma(x, y)$ can be written as a scalar product between $\boldsymbol{p}_\gamma(y)$ and $\hat{\boldsymbol{\gamma}}(x)$, that is,

$$\gamma(x, y) = \boldsymbol{p}_\gamma^T(y)\hat{\boldsymbol{\gamma}}(x), \tag{11}$$

where superscript T denotes transposition and $\hat{\boldsymbol{\gamma}} : l \to \mathbb{R}^m$ contains the functional coefficients as components. We emphasize that, once the profile vector $\boldsymbol{p}_\gamma(y)$ has been assigned, the field $\gamma(x, y)$ is uniquely determined by the components of $\hat{\boldsymbol{\gamma}}(x)$. Such components, for all the involved fields, are indeed the *unknowns* of the beam models we will develop. We also remark that, due to assumption (11), the computation of partial derivatives is straightforward, since:

$$\frac{\partial}{\partial x}\gamma = \frac{\partial}{\partial x}(\boldsymbol{p}_\gamma^T\hat{\boldsymbol{\gamma}}) = \boldsymbol{p}_\gamma^T\frac{d}{dx}\hat{\boldsymbol{\gamma}} = \boldsymbol{p}_\gamma^T\hat{\boldsymbol{\gamma}}', \qquad \frac{\partial}{\partial y}\gamma = \frac{\partial}{\partial y}(\boldsymbol{p}_\gamma^T\hat{\boldsymbol{\gamma}}) = \frac{d}{dy}\boldsymbol{p}_\gamma^T\hat{\boldsymbol{\gamma}} = \boldsymbol{p}_\gamma'^T\hat{\boldsymbol{\gamma}},$$

where we use a prime to indicate derivatives along both x and y, as there is no risk of confusion. Adopting the notation introduced in (11) and switching now to an engineering notation we set

$$\boldsymbol{s}(x, y) = \begin{Bmatrix} s_u(x, y) \\ s_v(x, y) \end{Bmatrix} = \begin{bmatrix} \boldsymbol{p}_u^T(y) & \boldsymbol{0} \\ \boldsymbol{0} & \boldsymbol{p}_v^T(y) \end{bmatrix} \begin{Bmatrix} \hat{\boldsymbol{u}}(x) \\ \hat{\boldsymbol{v}}(x) \end{Bmatrix} = \boldsymbol{P}_s\hat{\boldsymbol{s}}, \tag{12}$$

$$\boldsymbol{\sigma}(x, y) = \begin{Bmatrix} \sigma_{xx}(x, y) \\ \sigma_{yy}(x, y) \\ \tau_{xy}(x, y) \end{Bmatrix} = \begin{bmatrix} \boldsymbol{p}_{\sigma_x}^T(y) & \boldsymbol{0} & \boldsymbol{0} \\ \boldsymbol{0} & \boldsymbol{p}_{\sigma_y}^T(y) & \boldsymbol{0} \\ \boldsymbol{0} & \boldsymbol{0} & \boldsymbol{p}_\tau^T(y) \end{bmatrix} \begin{Bmatrix} \hat{\boldsymbol{\sigma}}_x(x) \\ \hat{\boldsymbol{\sigma}}_y(x) \\ \hat{\boldsymbol{\tau}}(x) \end{Bmatrix} = \boldsymbol{P}_\sigma\hat{\boldsymbol{\sigma}}, \tag{13}$$

where, for $\boldsymbol{P}_s$ and $\boldsymbol{P}_\sigma$ ($\hat{\boldsymbol{s}}$ and $\hat{\boldsymbol{\sigma}}$, respectively), we drop the explicit dependence on y (or x, respectively), for notational simplicity. The virtual fields are analogously defined as $\delta\boldsymbol{s} = \boldsymbol{P}_s\,\delta\hat{\boldsymbol{s}}$ and $\delta\boldsymbol{\sigma} = \boldsymbol{P}_\sigma\,\delta\hat{\boldsymbol{\sigma}}$.

In Section 3, $\boldsymbol{D}^{-1}$ denotes the fourth-order elastic tensor; from now on, we use the same notation to indicate the corresponding square matrix obtained following engineering notation. Therefore, we have

$$\boldsymbol{D}^{-1} = \frac{1}{E}\begin{bmatrix} 1 & -\nu & 0 \\ -\nu & 1 & 0 \\ 0 & 0 & 2(1+\nu) \end{bmatrix}.$$

4.2. ***Formulation of the problems.*** We consider the special case of a beam for which

$$\bar{\boldsymbol{s}} = \boldsymbol{0} \ \text{ on } A_0 = \partial\Omega_s, \qquad \boldsymbol{t} \neq \boldsymbol{0} \ \text{ on } A_l, \qquad \boldsymbol{f} = \boldsymbol{0} \ \text{ in } \Omega, \qquad \boldsymbol{t} = \boldsymbol{0} \ \text{ on } S_0 \cup S_n.$$

Hence, $\partial\Omega_t = A_l \cup S_0 \cup S_n$; the beam is clamped on the left-hand side A_0, and is subjected to a nonvanishing traction field on the right-hand side A_l. Furthermore, we suppose that $\boldsymbol{t}|_{A_l}$ can be exactly represented using the chosen profiles for $\boldsymbol{\sigma}\cdot\boldsymbol{n}$. Recalling (13), and noting that $\boldsymbol{n}|_{A_l} = (1,0)^T$, this means that there exist suitable vectors $\hat{\boldsymbol{t}}_x$ and $\hat{\boldsymbol{t}}_\tau$ such that

$$\boldsymbol{t} = \begin{Bmatrix} \boldsymbol{p}_{\sigma_x}^T \hat{\boldsymbol{t}}_x \\ \boldsymbol{p}_\tau^T \hat{\boldsymbol{t}}_\tau \end{Bmatrix}. \tag{14}$$

Therefore, the boundary condition $\boldsymbol{\sigma}\cdot\boldsymbol{n}|_{A_l} = \boldsymbol{t}$ may be written as (see (13))

$$\begin{Bmatrix} \hat{\sigma}_x(\bar{l}) \\ \hat{\boldsymbol{\tau}}(\bar{l}) \end{Bmatrix} = \begin{Bmatrix} \hat{\boldsymbol{t}}_x \\ \hat{\boldsymbol{t}}_\tau \end{Bmatrix}. \tag{15}$$

All these assumptions can be modified to cover more general cases; nonetheless, this simple model is already adequate to illustrate the method's capabilities.

4.2.1. *HR grad-grad approach.* In the notation of Section 4.1, the HR grad-grad stationarity (5) becomes

$$\delta J_{\mathrm{HR}}^{\mathrm{gg}} = \int_\Omega \Big[\Big(\frac{d}{dx}\boldsymbol{E}_1^T + \frac{d}{dy}\boldsymbol{E}_2^T\Big)\boldsymbol{P}_s\delta\hat{\boldsymbol{s}}\Big]^T \boldsymbol{P}_\sigma\hat{\boldsymbol{\sigma}}\,d\Omega + \int_\Omega \delta\hat{\boldsymbol{\sigma}}^T\boldsymbol{P}_\sigma^T\Big[\Big(\frac{d}{dx}\boldsymbol{E}_1^T + \frac{d}{dy}\boldsymbol{E}_2^T\Big)\boldsymbol{P}_s\hat{\boldsymbol{s}}\Big]d\Omega$$
$$- \int_\Omega \delta\hat{\boldsymbol{\sigma}}^T\boldsymbol{P}_\sigma^T\boldsymbol{D}^{-1}\boldsymbol{P}_\sigma\hat{\boldsymbol{\sigma}}\,d\Omega - \int_{\partial\Omega_t}\delta\hat{\boldsymbol{s}}^T\boldsymbol{P}_s^T\boldsymbol{t}\,dy = 0. \tag{16}$$

Expanding (16) we obtain

$$\delta J_{\mathrm{HR}}^{\mathrm{gg}} = \int_\Omega (\delta\hat{\boldsymbol{s}}'^T\boldsymbol{P}_s'^T\boldsymbol{E}_1\boldsymbol{P}_\sigma\hat{\boldsymbol{\sigma}} + \delta\hat{\boldsymbol{s}}^T\boldsymbol{P}_s'^T\boldsymbol{E}_2\boldsymbol{P}_\sigma\hat{\boldsymbol{\sigma}})\,d\Omega + \int_\Omega (\delta\hat{\boldsymbol{\sigma}}^T\boldsymbol{P}_\sigma^T\boldsymbol{E}_1^T\boldsymbol{P}_s\hat{\boldsymbol{s}}' + \delta\hat{\boldsymbol{\sigma}}^T\boldsymbol{P}_\sigma^T\boldsymbol{E}_2^T\boldsymbol{P}_s'\hat{\boldsymbol{s}})\,d\Omega$$
$$- \int_\Omega \delta\hat{\boldsymbol{\sigma}}^T\boldsymbol{P}_\sigma^T\boldsymbol{D}^{-1}\boldsymbol{P}_\sigma\hat{\boldsymbol{\sigma}}\,d\Omega - \int_{A_l}\delta\hat{\boldsymbol{s}}^T\boldsymbol{P}_s^T\boldsymbol{t}\,dy = 0. \tag{17}$$

Using the Fubini–Tonelli theorem, (17) can be written as

$$\delta J_{\mathrm{HR}}^{\mathrm{gg}} = \int_l (\delta\hat{\boldsymbol{s}}'^T\boldsymbol{G}_{s\sigma}\hat{\boldsymbol{\sigma}} + \delta\hat{\boldsymbol{s}}^T\boldsymbol{H}_{s'\sigma}\hat{\boldsymbol{\sigma}} + \delta\hat{\boldsymbol{\sigma}}^T\boldsymbol{G}_{\sigma s}\hat{\boldsymbol{s}}' + \delta\hat{\boldsymbol{\sigma}}^T\boldsymbol{H}_{\sigma s'}\hat{\boldsymbol{s}} - \delta\hat{\boldsymbol{\sigma}}^T\boldsymbol{H}_{\sigma\sigma}\hat{\boldsymbol{\sigma}})\,dx - \delta\hat{\boldsymbol{s}}^T\boldsymbol{T}_x\Big|_{x=\bar{l}} = 0, \tag{18}$$

where

$$\begin{aligned} \boldsymbol{G}_{s\sigma} &= \boldsymbol{G}_{\sigma s}^T = \int_A \boldsymbol{P}_s^T\boldsymbol{E}_1\boldsymbol{P}_\sigma\,dy, & \boldsymbol{H}_{\sigma\sigma} &= \int_A \boldsymbol{P}_\sigma^T\boldsymbol{D}^{-1}\boldsymbol{P}_\sigma\,dy, \\ \boldsymbol{H}_{s'\sigma} &= \boldsymbol{H}_{\sigma s'}^T = \int_A \boldsymbol{P}_s'^T\boldsymbol{E}_2\boldsymbol{P}_\sigma\,dy, & \boldsymbol{T}_x &= \int_{A_l}\boldsymbol{P}_s^T\boldsymbol{t}\,dy. \end{aligned} \tag{19}$$

Equation (18) represents the weak form of the 1D beam model. To obtain the corresponding boundary value problem, we integrate by parts the first term of (18):

$$\int_l \delta\hat{\boldsymbol{s}}'^T \boldsymbol{G}_{s\sigma}\hat{\boldsymbol{\sigma}}\,dx = \delta\hat{\boldsymbol{s}}^T \boldsymbol{G}_{s\sigma}\hat{\boldsymbol{\sigma}}|_{x=0}^{x=\bar{l}} - \int_l \delta\hat{\boldsymbol{s}}^T \boldsymbol{G}_{s\sigma}\hat{\boldsymbol{\sigma}}'\,dx. \tag{20}$$

Substituting (20) into (18), recalling that $\delta\hat{\boldsymbol{s}} = \boldsymbol{0}$ on A_0, and collecting the variables in a vector we obtain

$$\int_l [\delta\hat{\boldsymbol{s}};\, \delta\hat{\boldsymbol{\sigma}}]^T \left(\boldsymbol{G} \begin{Bmatrix} \hat{\boldsymbol{s}}' \\ \hat{\boldsymbol{\sigma}}' \end{Bmatrix} + \boldsymbol{H}^{\mathrm{gg}} \begin{Bmatrix} \hat{\boldsymbol{s}} \\ \hat{\boldsymbol{\sigma}} \end{Bmatrix} \right) dx + \delta\hat{\boldsymbol{s}}^T (\boldsymbol{G}_{s\sigma}\hat{\boldsymbol{\sigma}} - \boldsymbol{T}_x)|_{x=\bar{l}} = 0, \tag{21}$$

in which

$$\boldsymbol{G} = \begin{bmatrix} \boldsymbol{0} & -\boldsymbol{G}_{s\sigma} \\ \boldsymbol{G}_{\sigma s} & \boldsymbol{0} \end{bmatrix}, \qquad \boldsymbol{H}^{\mathrm{gg}} = \begin{bmatrix} \boldsymbol{0} & \boldsymbol{H}_{s'\sigma} \\ \boldsymbol{H}_{\sigma s'} & -\boldsymbol{H}_{\sigma\sigma} \end{bmatrix}. \tag{22}$$

Requiring that (21) is satisfied for all the possible variations and imposing the *essential* boundary condition $\hat{\boldsymbol{s}}$ we finally obtain

$$\boldsymbol{G} \begin{Bmatrix} \hat{\boldsymbol{s}}' \\ \hat{\boldsymbol{\sigma}}' \end{Bmatrix} + \boldsymbol{H}^{\mathrm{gg}} \begin{Bmatrix} \hat{\boldsymbol{s}} \\ \hat{\boldsymbol{\sigma}} \end{Bmatrix} = \begin{Bmatrix} \boldsymbol{0} \\ \boldsymbol{0} \end{Bmatrix} \quad \text{in } l, \qquad \boldsymbol{G}_{s\sigma}\hat{\boldsymbol{\sigma}} = \boldsymbol{T}_x \quad \text{at } x = \bar{l}, \qquad \hat{\boldsymbol{s}} = \boldsymbol{0} \quad \text{at } x = 0. \tag{23}$$

We remark that boundary value problem (23) is not necessarily well-posed. This depends on how the profile vectors have been chosen for all the involved fields. However, the well-posedness of (23) is guaranteed if the approximated fields are selected in accordance with the approximation theory of saddle-point problem (5) [Alessandrini et al. 1999].

4.2.2. *HR div-div approach.* Using the notation introduced in Section 4.1 in (7), the HR div-div functional stationarity becomes

$$\delta J_{\mathrm{HR}}^{\mathrm{dd}} = -\int_\Omega \delta\hat{\boldsymbol{s}}^T \boldsymbol{P}_s^T \left[\left(\frac{d}{dx}\boldsymbol{E}_1 + \frac{d}{dy}\boldsymbol{E}_2 \right) \boldsymbol{P}_\sigma \hat{\boldsymbol{\sigma}} \right] d\Omega - \int_\Omega \left[\left(\frac{d}{dx}\boldsymbol{E}_1 + \frac{d}{dy}\boldsymbol{E}_2 \right) \boldsymbol{P}_\sigma \delta\hat{\boldsymbol{\sigma}} \right]^T \boldsymbol{P}_s \hat{\boldsymbol{s}}\, d\Omega$$
$$- \int_\Omega \delta\hat{\boldsymbol{\sigma}}^T \boldsymbol{P}_\sigma^T \boldsymbol{D}^{-1} \boldsymbol{P}_\sigma \hat{\boldsymbol{\sigma}}\, d\Omega = 0. \tag{24}$$

Expanding (24), the weak formulation becomes

$$\delta J_{\mathrm{HR}}^{\mathrm{dd}} = -\int_\Omega (\delta\hat{\boldsymbol{s}}^T \boldsymbol{P}_s^T \boldsymbol{E}_1 \boldsymbol{P}_\sigma \hat{\boldsymbol{\sigma}}' + \delta\hat{\boldsymbol{s}}^T \boldsymbol{P}_s^T \boldsymbol{E}_2 \boldsymbol{P}'_\sigma \hat{\boldsymbol{\sigma}})\, d\Omega - \int_\Omega (\delta\hat{\boldsymbol{\sigma}}'^T \boldsymbol{P}_\sigma^T \boldsymbol{E}_1^T \boldsymbol{P}_s \hat{\boldsymbol{s}} + \delta\hat{\boldsymbol{\sigma}}^T \boldsymbol{P}'^T_\sigma \boldsymbol{E}_2^T \boldsymbol{P}_s \hat{\boldsymbol{s}})\, d\Omega$$
$$- \int_\Omega \delta\hat{\boldsymbol{\sigma}}^T \boldsymbol{P}_\sigma^T \boldsymbol{D}^{-1} \boldsymbol{P}_\sigma \hat{\boldsymbol{\sigma}}\, d\Omega = 0. \tag{25}$$

Again by the Fubini–Tonelli theorem, (25) becomes

$$\delta J_{\mathrm{HR}}^{\mathrm{dd}} = \int_l \left(-\delta\hat{\boldsymbol{s}}^T \boldsymbol{G}_{s\sigma}\hat{\boldsymbol{\sigma}}' - \delta\hat{\boldsymbol{s}}^T \boldsymbol{H}_{s\sigma'}\hat{\boldsymbol{\sigma}} - \delta\hat{\boldsymbol{\sigma}}'^T \boldsymbol{G}_{\sigma s}\hat{\boldsymbol{s}} - \delta\hat{\boldsymbol{\sigma}}^T \boldsymbol{H}_{\sigma' s}\hat{\boldsymbol{s}} - \delta\hat{\boldsymbol{\sigma}}^T \boldsymbol{H}_{\sigma\sigma}\hat{\boldsymbol{\sigma}} \right) dx = 0, \tag{26}$$

where

$$\boldsymbol{H}_{\sigma' s} = \boldsymbol{H}_{s\sigma'}^T = \int_A \boldsymbol{P}'^T_\sigma \boldsymbol{E}_2 \boldsymbol{P}_s\, dy$$

while the other matrices are as in (19).

Equation (26) represents the weak form of the 1D beam model. To obtain the corresponding boundary value problem, we integrate the third term by parts:

$$-\int_l \delta\hat{\boldsymbol{\sigma}}'^T \boldsymbol{G}_{\sigma s}\hat{\boldsymbol{s}}\,dx = -\delta\hat{\boldsymbol{\sigma}}^T \boldsymbol{G}_{\sigma s}\hat{\boldsymbol{s}}|_{x=0}^{x=\bar{l}} + \int_l \delta\hat{\boldsymbol{\sigma}}^T \boldsymbol{G}_{\sigma s}\hat{\boldsymbol{s}}'\,dx. \tag{27}$$

Substituting (27) into (26), recalling that $\boldsymbol{G}_{s\sigma}\delta\hat{\boldsymbol{\sigma}} = \boldsymbol{0}$ at $x = \bar{l}$, and collecting the unknowns in a vector we obtain

$$\int_l [\delta\hat{\boldsymbol{s}};\, \delta\hat{\boldsymbol{\sigma}}]^T \left(\boldsymbol{G} \begin{Bmatrix} \hat{\boldsymbol{s}}' \\ \hat{\boldsymbol{\sigma}}' \end{Bmatrix} + \boldsymbol{H}^{\mathrm{dd}} \begin{Bmatrix} \hat{\boldsymbol{s}} \\ \hat{\boldsymbol{\sigma}} \end{Bmatrix} \right) dx + \delta\hat{\boldsymbol{\sigma}}^T \boldsymbol{G}_{\sigma s}\hat{\boldsymbol{s}}|_{x=0} = 0, \tag{28}$$

where $\boldsymbol{G}$ is defined as in (22) and $\boldsymbol{H}^{\mathrm{dd}}$ is defined as

$$\boldsymbol{H}^{\mathrm{dd}} = \begin{bmatrix} \boldsymbol{0} & -\boldsymbol{H}_{s\sigma'} \\ -\boldsymbol{H}_{\sigma' s} & -\boldsymbol{H}_{\sigma\sigma} \end{bmatrix}. \tag{29}$$

Requiring that (28) be satisfied for all possible variations, and imposing the *essential* boundary condition (15), we finally obtain

$$\boldsymbol{G} \begin{Bmatrix} \hat{\boldsymbol{s}}' \\ \hat{\boldsymbol{\sigma}}' \end{Bmatrix} + \boldsymbol{H}^{\mathrm{dd}} \begin{Bmatrix} \hat{\boldsymbol{s}} \\ \hat{\boldsymbol{\sigma}} \end{Bmatrix} = \begin{Bmatrix} \boldsymbol{0} \\ \boldsymbol{0} \end{Bmatrix} \quad \text{in } l, \quad \hat{\boldsymbol{\sigma}}_x = \hat{\boldsymbol{t}}_x \ \text{ at } x = \bar{l}, \quad \hat{\boldsymbol{\tau}} = \hat{\boldsymbol{t}}_\tau \ \text{ at } x = \bar{l}, \quad \boldsymbol{G}_{\sigma s}\hat{\boldsymbol{s}} = \boldsymbol{0} \ \text{ at } x = 0. \tag{30}$$

We remark that boundary value problem (30) is not necessarily well-posed. This depends on how the profile vectors have been chosen for all the fields involved. However, (30) is guaranteed to be well-posed if the approximated fields are selected according to the approximation theory of the saddle-point problem (7); see [Alessandrini et al. 1999].

4.3. ***Conclusions on the derived beam models.*** From the development in this section, we can make the following remarks.

- Starting from different versions of the HR stationarity condition — grad-grad (5) and div-div (7) — and introducing hypothesis (11), we obtain two different classes of 1D beam models. Both classes may be described by a boundary value problem of the following type:

$$\boldsymbol{G} \begin{Bmatrix} \hat{\boldsymbol{s}}' \\ \hat{\boldsymbol{\sigma}}' \end{Bmatrix} + \boldsymbol{H} \begin{Bmatrix} \hat{\boldsymbol{s}} \\ \hat{\boldsymbol{\sigma}} \end{Bmatrix} = \begin{Bmatrix} \boldsymbol{0} \\ \boldsymbol{0} \end{Bmatrix} \qquad + \text{ suitable boundary conditions.} \tag{31}$$

  The difference between models based on the HR grad-grad and HR div-div formulations lies in the $\boldsymbol{H}$ matrix. More precisely:
  - $\boldsymbol{H} = \boldsymbol{H}^{\mathrm{gg}}$ for the HR grad-grad formulation. In this case, derivatives are applied to the displacement fields through the symmetric gradient operator, and the resulting models most likely strongly satisfy the compatibility law, though not necessarily the equilibrium equation.
  - $\boldsymbol{H} = \boldsymbol{H}^{\mathrm{dd}}$ for the HR div-div formulation. In this case, derivatives are applied to the stress fields through the divergence operator, and the resulting models most likely strongly satisfy the equilibrium equation, though not the necessarily the compatibility equation.
- The boundary value problem (30) can be explicitly written as

$$-\boldsymbol{G}_{s\sigma}\hat{\boldsymbol{\sigma}}' - \boldsymbol{H}_{s\sigma'}\hat{\boldsymbol{\sigma}} = \boldsymbol{0}, \qquad \boldsymbol{G}_{\sigma s}\hat{\boldsymbol{s}}' - \boldsymbol{H}_{\sigma' s}\hat{\boldsymbol{s}} - \boldsymbol{H}_{\sigma\sigma}\hat{\boldsymbol{\sigma}} = \boldsymbol{0} \qquad + \text{ suitable boundary conditions.}$$

We can compute $\hat{\boldsymbol{\sigma}}$ from the second equation and substitute it into the first, obtaining a displacement-like formulation of the problem:

$$\boldsymbol{A}\hat{\boldsymbol{s}}'' + \boldsymbol{B}\hat{\boldsymbol{s}}' + \boldsymbol{C}\hat{\boldsymbol{s}} = \boldsymbol{0} \qquad + \text{ suitable boundary conditions,} \tag{32}$$

where

$$\boldsymbol{A} = -\boldsymbol{G}_{s\sigma}\boldsymbol{H}_{\sigma\sigma}^{-1}\boldsymbol{G}_{\sigma s}, \quad \boldsymbol{B} = -\boldsymbol{G}_{s\sigma}\boldsymbol{H}_{\sigma\sigma}^{-1}\boldsymbol{H}_{\sigma' s} + \boldsymbol{H}_{s\sigma'}\boldsymbol{H}_{\sigma\sigma}^{-1}\boldsymbol{G}_{\sigma s}, \quad \boldsymbol{C} = \boldsymbol{H}_{s\sigma'}\boldsymbol{H}_{\sigma\sigma}^{-1}\boldsymbol{H}_{\sigma' s}.$$

Similar considerations apply to problem (23).

5. Examples of beam models

In this section we give two examples of beam models developed using the strategies of Section 4. More precisely, starting from the HR div-div approach in Equation (30), we derive

- a single layer beam model in which we use a first-order displacement field, thus showing that the approach under discussion is able to reproduce the classical models; and
- a multilayer beam model, in which we consider also higher-order kinematic and stress fields, thus illustrating how the approach can produce a refined model with a reasonable solution.

5.1. ***Single layer beam.*** Considering a homogeneous beam, we assume a first-order kinematic (as in the Timoshenko model) and the usual cross-section stress distributions (obtained from Jourawsky theory). In other words, we make the following hypotheses:

$$\begin{aligned}
&u = u_0(x) + y u_1(x), && \text{that is,} && \boldsymbol{p}_u = \{1 \;\; y\}^T, && \hat{\boldsymbol{u}} = \{u_0 \;\; u_1\}^T,\\
&v = v(x), && \text{that is,} && \boldsymbol{p}_v = \{1\}, && \hat{\boldsymbol{v}} = \{v\},\\
&\sigma_{xx} = \sigma_{x0}(x) + y\sigma_{x1}(x), && \text{that is,} && \boldsymbol{p}_{\sigma_x} = \{1 \;\; y\}^T, && \hat{\boldsymbol{\sigma}}_x = \{\sigma_{x0} \;\; \sigma_{x1}\}^T,\\
&\sigma_{yy} = 0, && \text{that is,} && \boldsymbol{p}_{\sigma_y} = \{0\}, && \hat{\boldsymbol{\sigma}}_y = \{0\},\\
&\tau = (1 - 4y^2/h^2)\tau(x), && \text{that is,} && \boldsymbol{p}_\tau = \{1 - 4y^2/h^2\}, && \hat{\boldsymbol{\tau}} = \{\tau\}.
\end{aligned}$$

The matrices $\boldsymbol{G}$ and $\boldsymbol{H}^{\mathrm{dd}}$ defined in (22) and (29), and entering into the beam model (30), are explicitly given by

$$\boldsymbol{G} = \begin{bmatrix}
0 & 0 & 0 & -h & 0 & 0\\
0 & 0 & 0 & 0 & -\frac{h^3}{12} & 0\\
0 & 0 & 0 & 0 & 0 & -\frac{2}{3}h\\
h & 0 & 0 & 0 & 0 & 0\\
0 & \frac{h^3}{12} & 0 & 0 & 0 & 0\\
0 & 0 & \frac{2}{3}h & 0 & 0 & 0
\end{bmatrix}, \qquad \boldsymbol{H}^{\mathrm{dd}} = \begin{bmatrix}
0 & 0 & 0 & 0 & 0 & 0\\
0 & 0 & 0 & 0 & 0 & \frac{2}{3}h\\
0 & 0 & 0 & 0 & 0 & 0\\
0 & 0 & 0 & -\frac{h}{E} & 0 & 0\\
0 & 0 & 0 & 0 & -\frac{h^3}{12}\frac{1}{E} & 0\\
0 & \frac{2}{3}h & 0 & 0 & 0 & -\frac{8}{15}h\frac{2(1+\nu)}{E}
\end{bmatrix}. \tag{33}$$

Since the problem (30) is governed by an ODE system with constant coefficients, the homogeneous

solution can be analytically computed. For example, choosing $h = 1\,\text{mm}$, $l = 10\,\text{mm}$, $E = 10^5\,\text{MPa}$, and $\nu = 0.25$, the homogeneous solution is given by

$$\begin{aligned} &u_0 = 5.00\cdot 10^{-6}C_4x + C_1, \qquad u_1 = 4.00\cdot 10^{-6}C_6x^2 + 5.00\cdot 10^{-6}C_5x + C_2,\\ &v = -(1.33\cdot 10^{-5}C_6x^3 + 5.00\cdot 10^{-6}C_5x^2 + 5.00\cdot 10^{-1}C_2x + C_3) + 10^{-5}C_6x,\\ &\sigma_{x0} = C_4, \qquad \sigma_{x1} = 4.00C_6x + C_5, \qquad \tau = C_6, \end{aligned} \tag{34}$$

in which the C_i are arbitrary constants, which may be determined by imposing the boundary conditions specified in (30). Indeed, for the beam model under consideration, the boundary conditions in (30) lead to a set of six linearly independent equations, since the matrix $\boldsymbol{G}_{\sigma s}$ of (19) and (22) is invertible.

We remark that the solution (34) is compatible with the one obtained by the Timoshenko beam model. However, we underline that the stress distributions along the beam axis are obtained directly from the model solution, and not by means of the displacement derivatives, as happens in classical formulations.

We also notice that, reducing the model to the displacement formulation (see (32)), we obtain the ODE system

$$\begin{gathered} hEu_0'' = 0, \qquad \frac{h^3}{12}Eu_1'' - \frac{5}{6}\frac{Eh}{2(1+\nu)}(v' + u_1) = 0, \qquad \frac{5}{6}\frac{Eh}{2(1+\nu)}(v'' + u_1') = 0\\ + \text{ suitable boundary conditions.} \end{gathered} \tag{35}$$

Not surprisingly, we again recover the classical Timoshenko equations, in which, however, the exact shear correction factor $\frac{5}{6}$ automatically appears. The same result holds true in the framework of variational plate modeling proposed in [Alessandrini et al. 1999].

5.2. ***Multilayered beam.*** We now consider a beam composed of n layers, as illustrated in Figure 2. The geometric and material parameters for the generic i-th layer are the thickness h_i, the Young's modulus E_i, and the Poisson ratio ν_i, collected in the n-dimensional vectors $\boldsymbol{h}$, $\boldsymbol{E}$, and $\boldsymbol{\nu}$.

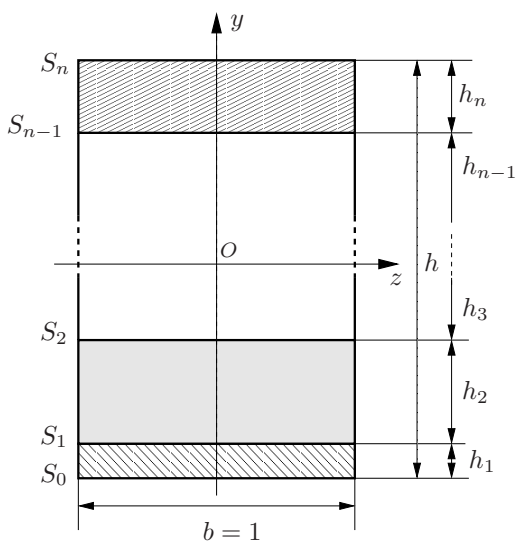

Figure 2. Cross-section geometry, coordinate system, dimensions, and adopted notations.

To design a multilayered beam model, we follow a two-step procedure:

(1) In each layer, we choose suitable profiles for every field involved in the modeling. Of course, given a generic field, the simplest choice, which we use here, is to use the same profiles for every layer.

(2) Across each interlayer, we impose the necessary continuity to ensure that the stresses belong to $H(\mathrm{div})$.

As a consequence, given a generic field γ, it is possible to define its profile vector $\boldsymbol{p}_\gamma$, which is characterized by

- the highest polynomial degree with respect to y used in a generic layer, denoted by $\deg \boldsymbol{p}_\gamma$, and
- regularity across each interlayer: continuity may or may not be required.

Since a main aim of this paper is to develop a model with an accurate stress description, a natural choice is to assume $\deg \boldsymbol{p}_\tau = 2$, as in Jourawsky theory. To ensure the well-posedness of the resulting model, we select the fields according to Table 2, where we also show the numbers of layer and global DOFs. Furthermore, we notice that we have to impose $\sigma_y = \tau = 0$ at the top and bottom of the beam.

Remark 5.1. More generally, to design a well-posed beam model one could choose

$$\deg \boldsymbol{p}_{\sigma_x} = \deg \boldsymbol{p}_u = \deg \boldsymbol{p}_\tau - 1, \qquad \deg \boldsymbol{p}_\tau = \deg \boldsymbol{p}_v = \deg \boldsymbol{p}_{\sigma_y} - 1, \tag{36}$$

together with the $H(\mathrm{div})$ regularity for the stress field.

5.2.1. *A test case.* We now present an easy case to test the robustness of the model: We consider a *homogeneous* beam, but treat it as if it were formed by three layers. The geometric and material properties are described by:

$$\boldsymbol{h} = \begin{Bmatrix} 0.300 \\ 0.367 \\ 0.333 \end{Bmatrix} \text{mm}, \qquad \boldsymbol{E} = \begin{Bmatrix} 10^5 \\ 10^5 \\ 10^5 \end{Bmatrix} \text{MPa}, \qquad \boldsymbol{\nu} = \begin{Bmatrix} 0.25 \\ 0.25 \\ 0.25 \end{Bmatrix}.$$

As a consequence, the total number of cross-section variables is 34. The boundary value problem (30) is uniquely solvable in this case. However, now the rank of $\boldsymbol{G}$ is 22, which means that (30) is actually a differential-algebraic boundary value problem. Thus, 22 variables are solutions of a differential problem, while the remaining 12 unknowns are algebraically determined by the former ones. We also remark that the boundary conditions in (30) actually lead to 22 independent constraints, since $\mathrm{rank}(\boldsymbol{G}_{\sigma s}) = 11$.

	$\deg \boldsymbol{p}_\gamma$	Interlayer continuity	Layer DOFs	Global DOFs
$\boldsymbol{p}_u$	1	no	2	$2n$
$\boldsymbol{p}_v$	2	no	3	$3n$
$\boldsymbol{p}_{\sigma_x}$	1	no	2	$2n$
$\boldsymbol{p}_{\sigma_y}$	3	yes	4	$3n-1$
$\boldsymbol{p}_\tau$	2	yes	3	$2n-1$

Table 2. Polynomial degrees of the profile vectors, continuity properties, and number of DOFs for a multilayered beam.

We now give the solution of the generalized eigenvalue problem $\det(\lambda \boldsymbol{G} + \boldsymbol{H}^{\mathrm{dd}}) = 0$, which goes into the construction of the homogeneous solution of (30):

$$\lambda = \left\{ \begin{array}{r} \sim 0 \\ 11.430 \pm 3.870i \\ -11.430 \pm 3.870i \\ 7.481 \pm 2.585i \\ -7.481 \pm 2.585i \\ 4.023 \pm 2.520i \\ -4.023 \pm 2.520i \\ 15.520 \pm 6.021i \\ -15.520 \pm 6.021i \end{array} \right\} \begin{array}{l} [6] \\ [1] \\ [1] \\ [1] \\ [1] \\ [1] \\ [1] \\ [1] \\ [1] \end{array}$$

where the numbers on the right are the eigenvalue multiplicities and the notation ~ 0 denotes eigenvalues that vanish up to the machine precision. We notice that the number of eigenvalues (22 in total) corresponds exactly to the rank of $\boldsymbol{G}$.

It is also possible to evaluate the homogeneous solution but, given the complexity of the problem, it is huge and we will not report it. Nevertheless it is possible to discuss its structure and make some important remarks:

- The zero eigenvalues lead to polynomial terms analogous to the Timoshenko homogeneous solution described in Section 5.1.
- The complex conjugate eigenvalues $(a \pm ib)$ lead to functions like $C_i e^{ax} \sin(bx + C_j)$, which describe local effects near the boundaries, as happens in several other beam models [Ladevèze and Simmonds 1998; Allix and Dupleix-Couderc 2009].

6. Numerical multilayered beam model

In this section we develop the FE corresponding to the multilayered beam model introduced in Section 5.2. This is equivalent to introducing a dimension reduction also along the beam axis, which leads to a purely algebraic system. The discretization of the axial fields $\hat{\boldsymbol{s}}$ and $\hat{\boldsymbol{\sigma}}$ can be generally described by

$$\begin{aligned} \hat{\boldsymbol{s}}(x) &\approxeq \boldsymbol{N}_s \tilde{\boldsymbol{s}} = \begin{bmatrix} \boldsymbol{N}_u(x) & \boldsymbol{0} \\ \boldsymbol{0} & \boldsymbol{N}_v(x) \end{bmatrix} \begin{Bmatrix} \tilde{\boldsymbol{u}} \\ \tilde{\boldsymbol{v}} \end{Bmatrix}, \qquad \hat{\boldsymbol{\sigma}}(x) \approxeq \boldsymbol{N}_\sigma \tilde{\boldsymbol{\sigma}} = \begin{bmatrix} \boldsymbol{N}_{\sigma_x}(x) & \boldsymbol{0} & \boldsymbol{0} \\ \boldsymbol{0} & \boldsymbol{N}_{\sigma_y}(x) & \boldsymbol{0} \\ \boldsymbol{0} & \boldsymbol{0} & \boldsymbol{N}_\tau(x) \end{bmatrix} \begin{Bmatrix} \tilde{\boldsymbol{\sigma}}_x \\ \tilde{\boldsymbol{\sigma}}_y \\ \tilde{\boldsymbol{\tau}} \end{Bmatrix}, \\ \hat{\boldsymbol{s}}'(x) &\approxeq \boldsymbol{B}_s \tilde{\boldsymbol{s}} = \begin{bmatrix} \boldsymbol{N}'_u(x) & \boldsymbol{0} \\ \boldsymbol{0} & \boldsymbol{N}'_v(x) \end{bmatrix} \begin{Bmatrix} \tilde{\boldsymbol{u}} \\ \tilde{\boldsymbol{v}} \end{Bmatrix}, \qquad \hat{\boldsymbol{\sigma}}'(x) \approxeq \boldsymbol{B}_\sigma \tilde{\boldsymbol{\sigma}} = \begin{bmatrix} \boldsymbol{N}'_{\sigma_x}(x) & \boldsymbol{0} & \boldsymbol{0} \\ \boldsymbol{0} & \boldsymbol{N}'_{\sigma_y}(x) & \boldsymbol{0} \\ \boldsymbol{0} & \boldsymbol{0} & \boldsymbol{N}'_\tau(x) \end{bmatrix} \begin{Bmatrix} \tilde{\boldsymbol{\sigma}}_x \\ \tilde{\boldsymbol{\sigma}}_y \\ \tilde{\boldsymbol{\tau}} \end{Bmatrix}. \end{aligned} \tag{37}$$

From now on, for notational simplicity, we will drop the explicit dependency on x for fields.

6.1. ***Weak problem formulation.*** We now make explicit the weak formulation we will use as a starting point for the FE discretization. To this end, we first recall the beam model variational formulation (26). Then, we integrate by parts with respect to the x direction both the first and third terms of (26). We thus

obtain: *Find* $\hat{\boldsymbol{s}} \in \tilde{W}$ *and* $\hat{\boldsymbol{\sigma}} \in \tilde{S}$ *such that, for every* $\delta\hat{\boldsymbol{s}} \in \tilde{W}$ *and for every* $\delta\hat{\boldsymbol{\sigma}} \in \tilde{S}$,

$$\delta J_{\mathrm{HR}} = \int_l (\delta\hat{\boldsymbol{s}}'^T \boldsymbol{G}_{s\sigma}\hat{\boldsymbol{\sigma}} - \delta\hat{\boldsymbol{s}}^T \boldsymbol{H}_{s\sigma'}\hat{\boldsymbol{\sigma}} + \delta\hat{\boldsymbol{\sigma}}^T \boldsymbol{G}_{\sigma s}\hat{\boldsymbol{s}}' - \delta\hat{\boldsymbol{\sigma}}^T \boldsymbol{H}_{\sigma' s}\hat{\boldsymbol{s}} - \delta\hat{\boldsymbol{\sigma}}^T \boldsymbol{H}_{\sigma\sigma}\hat{\boldsymbol{\sigma}})\,dx - \delta\hat{\boldsymbol{s}}^T \boldsymbol{T}_x|_{x=\bar{l}} = 0, \quad (38)$$

where $\tilde{W} := \{\hat{\boldsymbol{s}} \in H^1(l) : \hat{\boldsymbol{s}}|_{x=0} = \boldsymbol{0}\}$ and $\tilde{S} := L^2(l)$.

Notice that all the derivatives with respect to x are applied to displacement variables, whereas the derivatives with respect to y (incorporated into the $\boldsymbol{H}$ matrices) are applied to cross-section stress vectors. The resulting variational formulation has the following features:

- The obtained weak formulation (38) is symmetric.
- y-derivatives applied to stresses and the essential conditions of S_t^{dd} (see Section 3.2.2) most likely lead to a formulation which accurately solves the equilibrium equation in the y direction, that is, in the cross-section.
- x derivatives applied to displacements and the essential condition in $\tilde{W}$ most likely lead to a formulation which accurately solves the compatibility equation along the beam axis.

The FE discretization simply follows from the application of (37) to the variational formulation (38):

$$\begin{aligned}\delta J_{\mathrm{HR}} = \int_l \big(\delta\tilde{\boldsymbol{s}}^T \boldsymbol{B}_s^T \boldsymbol{G}_{s\sigma}\boldsymbol{N}_\sigma\tilde{\boldsymbol{\sigma}} - \delta\tilde{\boldsymbol{s}}^T \boldsymbol{N}_s^T \boldsymbol{H}_{s\sigma'}\boldsymbol{N}_\sigma\tilde{\boldsymbol{\sigma}} + \delta\tilde{\boldsymbol{\sigma}}^T \boldsymbol{N}_\sigma^T \boldsymbol{G}_{\sigma s}\boldsymbol{B}_s\tilde{\boldsymbol{s}}'\big)\,dx \\ - \int_l \big(\delta\tilde{\boldsymbol{\sigma}}^T \boldsymbol{N}_\sigma^T \boldsymbol{H}_{\sigma' s}\boldsymbol{N}_s\tilde{\boldsymbol{s}} + \delta\tilde{\boldsymbol{\sigma}}^T \boldsymbol{N}_\sigma^T \boldsymbol{H}_{\sigma\sigma}\boldsymbol{N}_\sigma\tilde{\boldsymbol{\sigma}}\big)\,dx - \delta\tilde{\boldsymbol{s}}^T \boldsymbol{N}_s^T \boldsymbol{T}_x|_{x=\bar{l}} = 0. \quad (39)\end{aligned}$$

Collecting unknown coefficients in a vector and requiring (39) to be satisfied for all possible virtual fields we obtain

$$\begin{bmatrix} \boldsymbol{0} & \boldsymbol{K}_{s\sigma} \\ \boldsymbol{K}_{\sigma s} & \boldsymbol{K}_{\sigma\sigma} \end{bmatrix} \begin{Bmatrix} \tilde{\boldsymbol{s}} \\ \tilde{\boldsymbol{\sigma}} \end{Bmatrix} = \begin{Bmatrix} \tilde{\boldsymbol{T}} \\ \boldsymbol{0} \end{Bmatrix}, \quad (40)$$

where

$$\boldsymbol{K}_{s\sigma} = \boldsymbol{K}_{\sigma s}^T = \int_l (\boldsymbol{B}_s^T \boldsymbol{G}_{s\sigma}\boldsymbol{N}_\sigma - \boldsymbol{N}_s^T \boldsymbol{H}_{s\sigma'}\boldsymbol{N}_\sigma)\,dx, \qquad \boldsymbol{K}_{\sigma\sigma} = -\int_l \boldsymbol{N}_\sigma^T \boldsymbol{H}_{\sigma\sigma}\boldsymbol{N}_\sigma\,dx, \qquad \tilde{\boldsymbol{T}} = \boldsymbol{N}_s^T \boldsymbol{T}_x|_{x=\bar{l}}.$$

In what follows we will focus, for all variables involved, on the finite element spaces shown in Table 3; we also recall the profile properties which have led to the multilayered beam model. For the polynomial degrees and continuity requirements we use the same notation as in Section 5.2. Thus, for example, the field v is approximated by means of piecewise cubic polynomials, continuous along the axial direction.

	deg $\boldsymbol{p}_\gamma$	y continuity	deg $\boldsymbol{N}_\gamma$	x continuity
u	1	no	2	yes
v	2	no	3	yes
σ_x	1	no	1	no
σ_y	3	yes	3	no
τ	2	yes	2	no

Table 3. Degree and continuity properties of shape functions with respect to the y and x directions.

We remark that this choice of the FE shape functions assures the stability and convergence of the resulting discrete scheme. We also notice that the stresses are discontinuous across elements along the x direction, so that it is possible to statically condensate them out at the element level, reducing the dimension of the global stiffness matrix and improving efficiency.

6.2. ***Multilayered homogeneous beam.*** We now consider the same three layer homogeneous beam of Section 5.2.1. Together with the clamping condition in A_0, we assume that $\bar{l} = 10\,\text{mm}$ and the beam is loaded along A_l by the quadratic shear stress distribution $\boldsymbol{t}|_{A_l} = [0, 3/2(1-4y^2)]^T$ MPa.

6.2.1. *Convergence.* In Table 4 we report on the mean value of the transverse displacement along A_l, as obtained by employing (a) the classical Euler–Bernoulli beam model; (b) the classical Timoshenko beam model; (c) the numerical model under investigation, in which the solution is computed using a mesh of 64 elements; (d) a 2D FE scheme in ABAQUS, using a fine regular grid of 3500×350 elements.

Due to the large number of elements used, we consider the latter solution as the reference solution, and we denote with v_{ex} its mean value along A_l.

In Table 4 we also report the relative error, defined by

$$e_{\text{rel}} = \frac{|v - v_{\text{ex}}|}{|v_{\text{ex}}|}, \tag{41}$$

where v is the mean value along A_l computed by the various procedures. This e_{rel} gives an indication of the accuracy of the model, even though it is not the usual error measure in terms of the natural norms.

Table 4 shows the superior performance of the three-layered mixed FE with respect to the other 1D models considered.

In Figure 3 we study the convergence of our numerical model. More precisely, we plot the relative quantity defined in (41), evaluated considering different mesh sizes δ in the x direction, and i layers of thickness $h_i = 1/i$, for $i = 1, 3, 5, 7$. From Figure 3a we notice that:

- using even a few elements the quantity e_{rel} is under 1%;
- the error e_{rel} decreases as the number of layers increases;
- using a highly refined mesh, the relative error e_{rel} increases, even as it apparently converges to a constant close to 10^{-3}. This behavior can be explained by recalling that *a modeling error* necessarily arises. Indeed, the solution of the 2D elastic problem and the solution of the multilayered beam mixed model do differ from each other, for a fixed length and thickness of the beam.

Beam theory	v [10^{-2} mm]	e_{rel} [10^{-3}]
Euler–Bernoulli	4.000000	6.192
Timoshenko	4.030000	1.261
Three-layered mixed FE	4.026460	0.382
2D solution	4.024924	

Table 4. Transverse displacements and relative errors of the free edge of a cantilever ($\bar{l} = 10\,\text{mm}$ and $h = 1\,\text{mm}$) obtained by different beam theories.

In Figure 3b we consider another relative quantity, e^*_{rel}, similar to that defined in (41), but using as the reference solution the one obtained by FE analysis of the multilayered model using the most refined x-direction mesh. We notice that: the sequences of errors e^*_{rel} converge monotonically to zero; and for a fixed number of layers, the log-log plots of errors suggest a convergence rate of the order of α, with $\alpha \approx 1$.

Finally, in Figure 3c we plot the relative error e_{rel} versus the number of layers (with the results obtained using a mesh of 32 elements). It is evident that the relative error decreases when incrementing the number of layers even if the succession is not linear.

6.2.2. *Boundary effects.* As already noticed in Section 5.2.1, the model under investigation is capable of capturing some local effects near the clamped boundary; we here present some results focused on that issue. Even though this study is far from being exhaustive, it gives an indication of the model's potential. In what follows the computations are performed using a mesh of 64 elements. To highlight the boundary

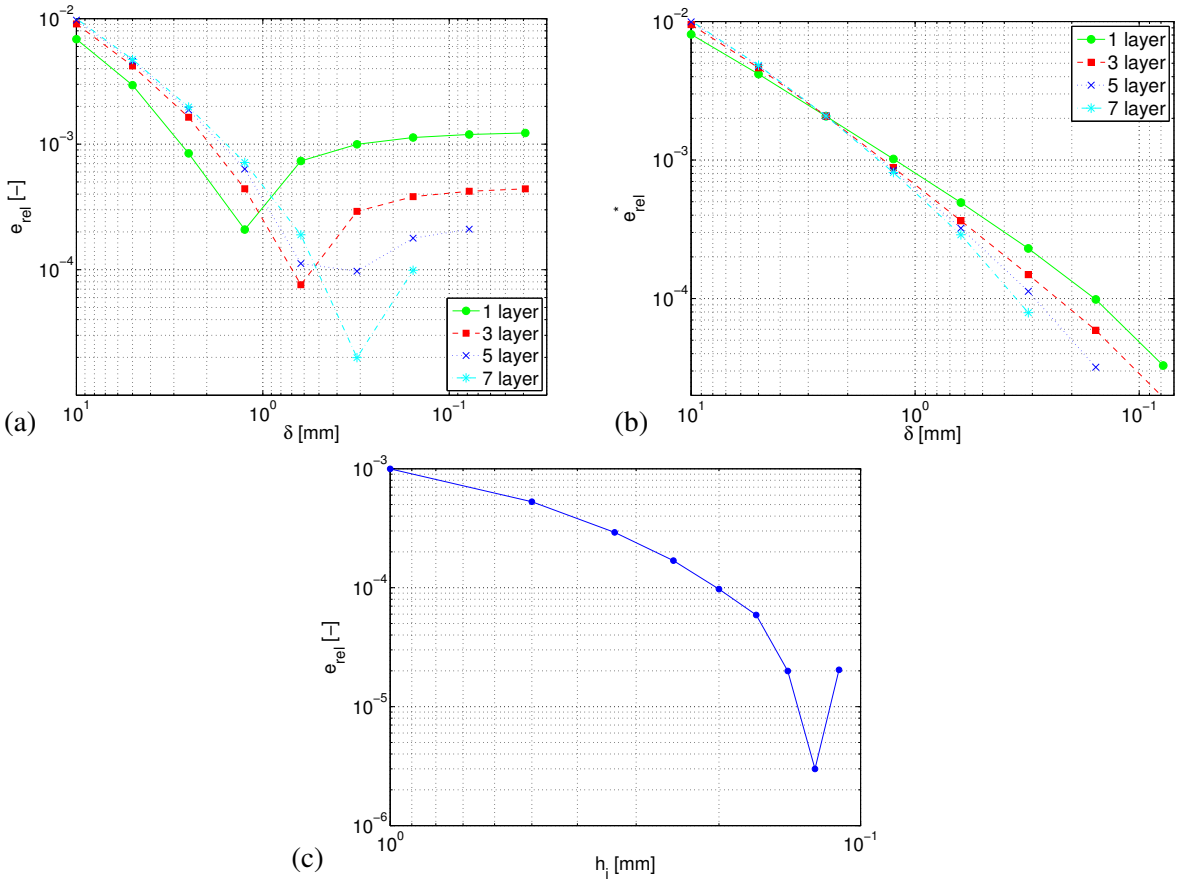

Figure 3. Relative errors on free-edge and transverse displacement for different mesh sizes δ and different numbers of layers. (a) Relative error e_{rel}, evaluated assuming v_{ex} is the 2D numerical solution. (b) Relative error e^*_{rel}, evaluated assuming v_{ex} is the 1D numerical solution obtained using the most refined x-direction mesh. (c) Relative error, plotted as a function of the layer thickness h_i, with mesh size $\delta = 0.3125$ mm.

effects we consider a beam analogous to the one introduced at the beginning of Section 6.2 in which we set $\bar{l} = 2.5$ mm. The results are reported in Figures 4, 5, and 6. We can appreciate the following:

- Far from the boundary, it is possible to recognize the classical beam solution: constant shear stress $\tau(x)$, linear axial stress $\sigma_x(x)$, quadratic horizontal displacement $u(x)$, and cubic transverse displacement $v(x)$.
- As expected, boundary effects decay as damped harmonic functions.
- The local effects decay very rapidly, so that only the first oscillation is significant. This result is consistent with the other models capable of capturing these kind of boundary effects.

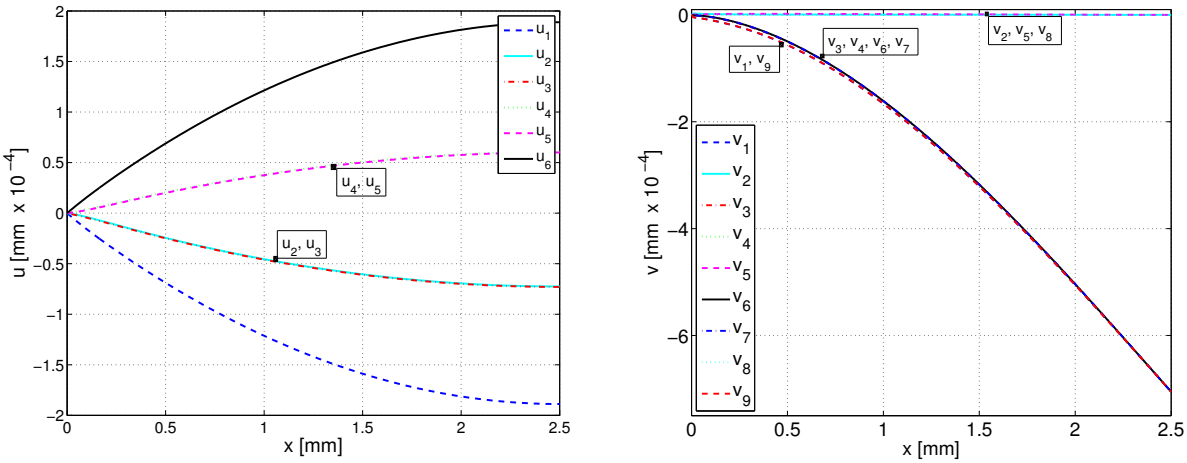

Figure 4. Axial displacements $\hat{\boldsymbol{u}}$ (left) and transverse displacements $\hat{\boldsymbol{v}}$ (right) as functions of x for a three-layer homogeneous cantilever, clamped at $x = 0$, loaded at $x = 2.5$ by a quadratic shear distribution, and modeled with 64 elements.

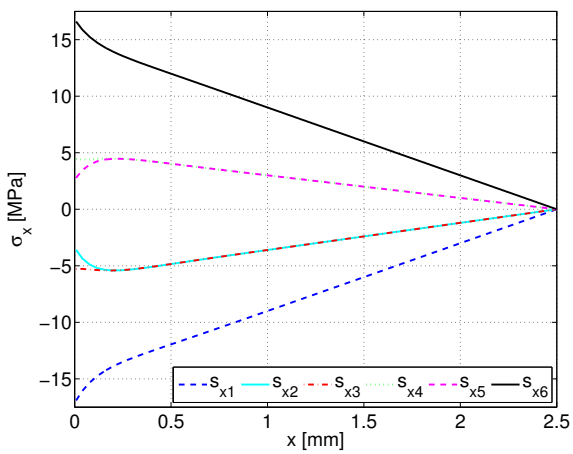

Figure 5. Axial stress $\hat{\boldsymbol{\sigma}}_x(x)$ of a three-layer homogeneous cantilever, clamped at $x = 0$, loaded at $x = 2.5$ by a quadratic shear distribution, and modeled with 64 elements.

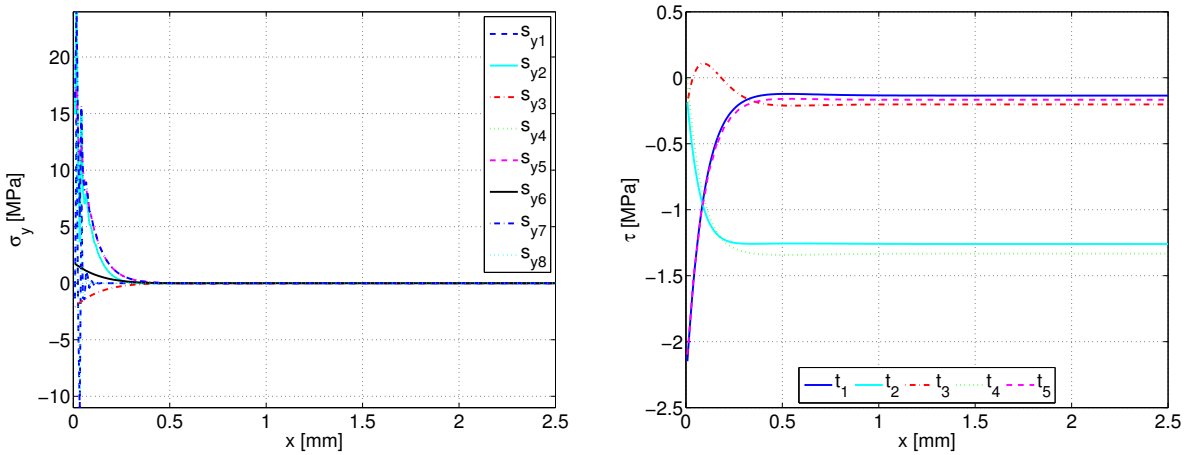

Figure 6. Transverse compressive stress $\hat{\sigma}_y$ (left) and shear stress $\hat{\tau}$ (right) as functions of x for a three-layer homogeneous cantilever, clamped at $x = 0$, loaded at $x = 2.5$ by a quadratic shear distribution, and modeled with 64 elements.

- Section striction, described by the quadratic displacement terms v_2, v_5, and v_8, is negligible, as assumed in first-order theories.

As specified in Table 3, in the numerical model under discussion we do not a priori impose displacement continuity across layers. In Figure 7 we plot the jump of the displacement filed across the interlayer surfaces S_1 and S_2. Figure 7, right, highlights that the transverse displacement jump rapidly decays far from the clamped boundary. On the other hand, from the left half of the figure we see that, far from the clamped boundary, the axial displacement jump $|u(x)^+ - u(x)^-|$ tends to a value different from zero (of the order of 10^{-7} mm). However, we notice that the displacement field is much greater, since it is of the order of 10^{-4} mm.

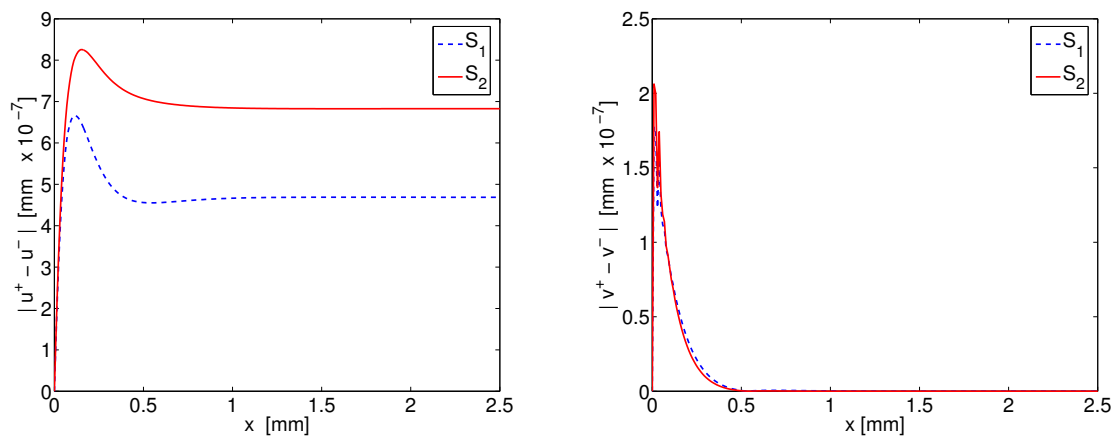

Figure 7. Compatibility mismatches on interlayer surfaces $y = -\frac{1}{5}$ (labeled S_1) and $y = \frac{1}{6}$ (S_2): axial displacement jump $|u(x)^+ - u(x)^-|$ (left) and transverse displacement jump $|v(x)^+ - v(x)^-|$ (right).

6.3. ***Multilayered nonhomogeneous beams.*** We now consider two nonhomogeneous beams. focusing particularly on the cross-section stress distributions, since such quantities are only seldom accurately captured in classical beam models.

6.3.1. *Symmetric section.* Figure 8 plots the stress distributions at different sections ($x = 2.5$, 0.5, and 0.125) calculated for a cantilever composed of three layers, clamped at A_0, for which $\bar{l} = 5$ mm and

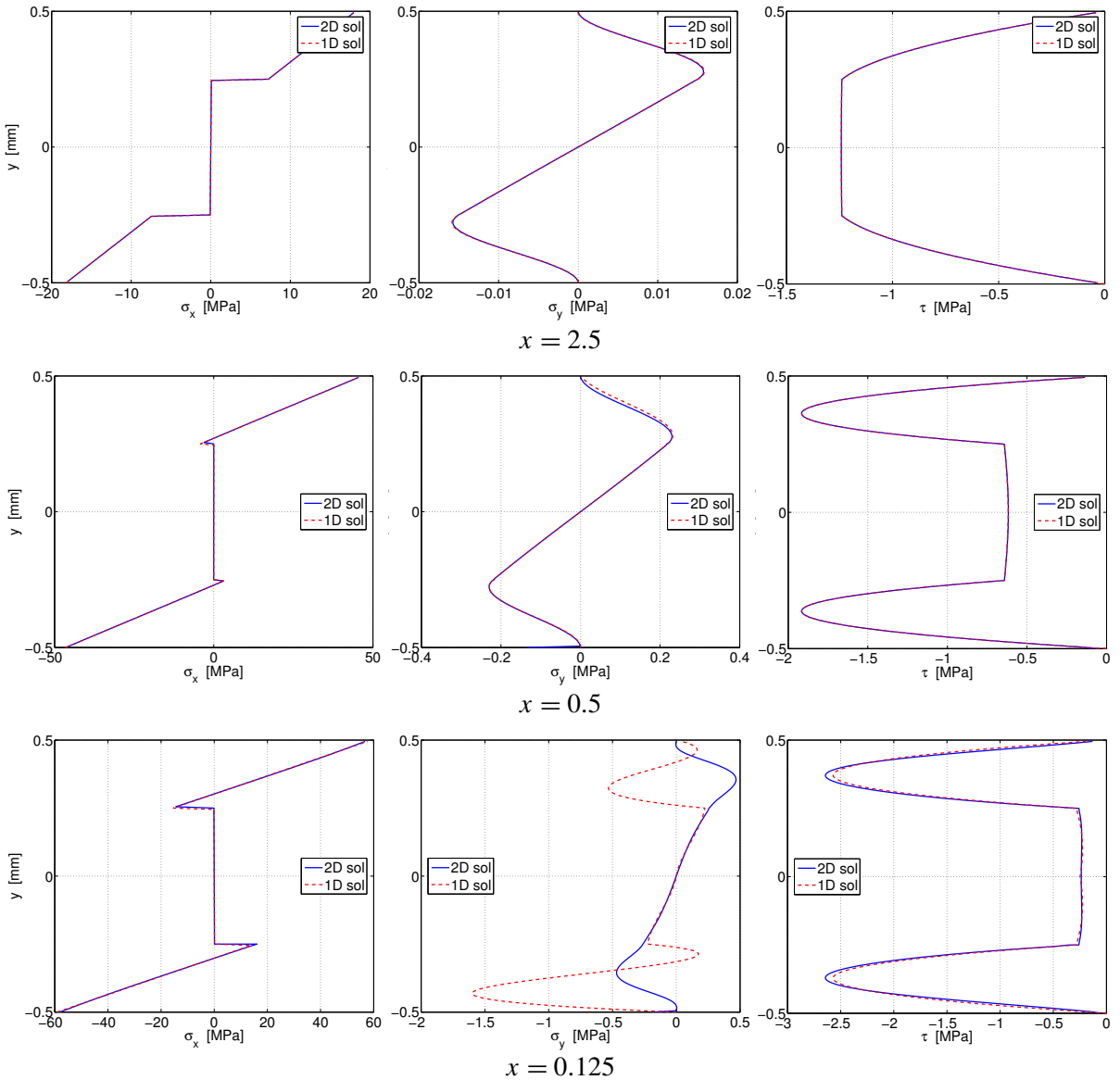

Figure 8. Cross-section stresses σ_x (left), σ_y (middle), and τ (right), as functions of y: one- and two-dimensional solutions for the symmetric section. Three cross-sections are considered, at various distances from the clamped boundary: far ($x = -2.5$, top), close ($x = 0.5$, middle), and very close ($x = 0.125$, bottom).

$\boldsymbol{t}|_{A_l} = \left[0, \frac{3}{2}(1-4y^2)\right]^T$ MPa, and whose geometry and mechanical properties are specified by

$$\boldsymbol{h} = \begin{Bmatrix} 0.25 \\ 0.50 \\ 0.25 \end{Bmatrix} \text{mm}, \qquad \boldsymbol{E} = \begin{Bmatrix} 1\cdot 10^5 \\ 1\cdot 10^3 \\ 1\cdot 10^5 \end{Bmatrix} \text{MPa}, \qquad \boldsymbol{\nu} = \begin{Bmatrix} 0.25 \\ 0.25 \\ 0.25 \end{Bmatrix}.$$

The solution of the 1D model was evaluated with a mesh size of $\delta = 0.15625$ mm (32 elements), and the 2D solution using ABAQUS with a mesh of 200×1000 square elements.

The ability of the numerical model to reproduce the stress distribution very accurately, far from the clamped boundary, is clearly seen from the top row of Figure 8. A similar feature is also maintained close to the clamped boundary (middle and bottom rows), even though some error progressively arises as we approach $x = 0$. In particular, the axial stress σ_x and the shear stress τ are very accurately described, whereas the σ_y approximation exhibits a worse performance (maybe also because some kind of instability arises; see Figure 6, left).

6.3.2. *Nonsymmetric section.* Figure 9 plots the stress distributions at the section $x = 2.5$ calculated for a cantilever composed of four layers, clamped at A_0, for which $\bar{l} = 5$ mm and $t = \ldots$ and whose geometric and mechanical properties of the section are specified by

$$\boldsymbol{h} = \begin{Bmatrix} 0.25 \\ 0.25 \\ 0.25 \\ 0.25 \end{Bmatrix} \text{mm}, \qquad \boldsymbol{E} = \begin{Bmatrix} 1\cdot 10^5 \\ 1\cdot 10^3 \\ 1\cdot 10^5 \\ 1\cdot 10^3 \end{Bmatrix} \text{MPa}, \qquad \boldsymbol{\nu} = \begin{Bmatrix} 0.25 \\ 0.25 \\ 0.25 \\ 0.25 \end{Bmatrix}.$$

We evaluate the 1D and 2D solutions using the same meshes as for the symmetric case just discussed.

As in the symmetric case, there is no significant difference between the 1D and the 2D cross-section stress distributions. We only notice a small deviation (below 1%) in the plot of σ_y.

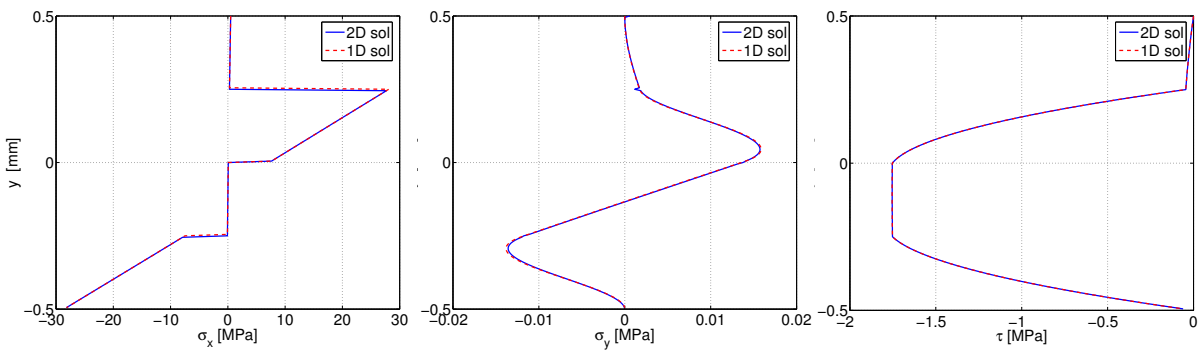

Figure 9. Cross-section stresses σ_x (left), σ_y (middle), and τ (right), as functions of y: one- and two-dimensional solutions for the nonsymmetric section.

7. Conclusions

In this paper we developed planar beam models based on dimension reduction by a variational approach. More precisely, we selected a suitable variational formulation among the ones available in the literature.

Our choice of the variational principle was motivated by the need to accurately describe the stress profiles. In Sections 4 and 5 we gave the general derivation of the beam models, together with a couple of examples. In Section 6 we focused on the multilayered model introduced in Section 5, for which we developed an efficient finite element scheme, as assessed by the presented numerical results.

Future developments of this work could include rigorous mathematical study of the models, generalization to 3D beams with variable cross-section, and the treatment of more sophisticated constitutive laws.

References

[Alessandrini et al. 1999] S. M. Alessandrini, D. N. Arnold, R. S. Falk, and A. L. Madureira, "Derivation and justification of plate models by variational methods", pp. 1–20 in *Plates and shells* (Quebec, 1996), edited by M. Fortin, CRM Proc. Lecture Notes **21**, Amer. Math. Soc., Providence, RI, 1999.

[Allix and Dupleix-Couderc 2009] O. Allix and C. Dupleix-Couderc, "A plate theory as a mean to compute precise 3D solutions including edge effects and related issues", *New Trends in Thin Structures* **519** (2009), 1–28.

[Auricchio and Sacco 1999] F. Auricchio and E. Sacco, "A mixed-enhanced finite-element for the analysis of laminated composite plates", *Int. J. Numer. Methods Eng.* **44** (1999), 1481–1504.

[Auricchio et al. 2004] F. Auricchio, C. Lovadina, and A. L. Madureira, "An asymptotically optimal model for isotropic heterogeneous linearly elastic plates", *M2AN Math. Model. Numer. Anal.* **38**:5 (2004), 877–897.

[Carrera 2000] E. Carrera, "Assessment of mixed and classical theories on global and local response of multilayered orthotropic plates", *Compos. Struct.* **50** (2000), 183–198.

[Carrera 2001] E. Carrera, "Developments, ideas and evaluations based upon Reissner's mixed variational theorem in the modeling of multilayered plates and shells", *Applied Mechanics Review* **54** (2001), 301–329.

[Carrera and Demasi 2002] E. Carrera and L. Demasi, "Classical and advanced multilayered plate elements based upon PVD and RMVT, 1: derivation of finite element matrices", *Int. J. Numer. Methods Eng.* **55**:2 (2002), 191–231.

[Demasi 2009a] L. Demasi, "Mixed plate theories based on the generalized unified formulation, I: governing equations", *Compos. Struct.* **87** (2009), 1–11.

[Demasi 2009b] L. Demasi, "Mixed plate theories based on the generalized unified formulation, II: layerwise theories", *Compos. Struct.* **87** (2009), 12–22.

[Demasi 2009c] L. Demasi, "Mixed plate theories based on the generalized unified formulation, III: advanced mixed high order shear deformation theories", *Compos. Struct.* **87** (2009), 183–194.

[Demasi 2009d] L. Demasi, "Mixed plate theories based on the generalized unified formulation, IV: zig-zag theories", *Compos. Struct.* **87** (2009), 195–205.

[Demasi 2009e] L. Demasi, "Mixed plate theories based on the generalized unified formulation, V: results", *Compos. Struct.* **88** (2009), 1–16.

[Feng and Hoa 1998] W. Feng and S. V. Hoa, "Partial hybrid finite elements for composite laminates", *Finite Elem. Anal. Des.* **30** (1998), 365–382.

[Hjelmstad 2005] K. D. Hjelmstad, *Fundamentals of structural mechanics*, Springer, 2005.

[Huang et al. 2002] Y. Huang, S. Di, C. Wu, and H. Sun, "Bending analysis of composite laminated plates using a partially hybrid stress element with interlaminar continuity", *Comput. Struct.* **80** (2002), 403–410.

[Icardi and Atzori 2004] U. Icardi and A. Atzori, "Simple, efficient mixed solid element for accurate analysis of local effects in laminated and sandwich composites", *Adv. Engng. Software* **35** (2004), 843–859.

[Ladevèze and Simmonds 1998] P. Ladevèze and J. Simmonds, "New concepts for linear beam theory with arbitrary geometry and loading", *Eur. J. Mech. A Solids* **17**:3 (1998), 377–402.

[Lo et al. 1977a] K. H. Lo, R. M. Christensen, and E. M. Wu, "A high order theory for plate deformations, I: homogeneous plates", *J. Appl. Mech.* (*ASME*) **44** (1977), 663–668.

[Lo et al. 1977b] K. H. Lo, R. M. Christensen, and E. M. Wu, "A high order theory for plate deformations, II: laminated plates", *J. Appl. Mech.* (*ASME*) **44** (1977), 669–676.

[Reddy 1984] J. N. Reddy, "A simple higher-order theory of laminated composite plates", *ASME, Journal of Applied Mechanics of Composite Materials* **51** (1984), 745–752.

[Reissner 1986] E. Reissner, "On a variational theorem and on shear deformable plate theory", *Int. J. Numer. Methods Eng.* **23** (1986), 193–198.

[Rohwer and Rolfes 1998] K. Rohwer and R. Rolfes, "Calculating 3D stresses in layered composite plates and shells", *Mech. Compos. Mater.* **34** (1998), 355–362.

[Rohwer et al. 2005] K. Rohwer, S. Friedrichs, and C. Wehmeyer, "Analyzing laminated structures from fiber-reinforced composite material — an assessment", *Tech. Mech.* **25** (2005), 59–79.

[Sheinman 2001] I. Sheinman, "On the analytical closed-form solution of high-order kinematic models in laminated beam theory", *Int. J. Numer. Methods Eng.* **50** (2001), 919–936.

[Spilker 1982] R. L. Spilker, "Hybrid-stress eight-node elements for thin and thick multilayer laminated plates", *Int. J. Numer. Methods Eng.* **18** (1982), 801–828.

[Timoshenko 1955] S. Timoshenko, *Strength of materials, I: elementary theory and problems*, 3rd ed., Van Nostrand, New York, 1955.

[Vinayak et al. 1996a] R. U. Vinayak, G. Prathap, and B. P. Naganarayana, "Beam elements based on a higher order theory, I: formulation and analysis of performance", *Comput. Struct.* **58** (1996), 775–789.

[Vinayak et al. 1996b] R. U. Vinayak, G. Prathap, and B. P. Naganarayana, "Beam elements based on a higher order theory, II: boundary layer sensitivity and stress oscillations", *Comput. Struct.* **58** (1996), 791–796.

[Wanji and Zhen 2008] C. Wanji and W. Zhen, "A selective review on recent development of displacement-based laminated plate theories", *Recent Patents Mech. Engng.* **1** (2008), 29–44.

Received 3 Dec 2009. Revised 1 Jun 2010. Accepted 16 Jun 2010.

FERDINANDO AURICCHIO: auricchio@unipv.it
Dipartimento di Meccanica Strutturale, Università degli Studi di Pavia, Via Ferrata 1, 27100 Pavia, Italy
http://www.unipv.it/auricchio/

GIUSEPPE BALDUZZI: giuseppe.balduzzi@unipv.it
Dipartimento di Meccanica Strutturale / Dipartimento di Matematica, Università degli Studi di Pavia, Via Ferrata 1, 27100 Pavia, Italy
http://www-2.unipv.it/compmech/members/giuseppebalduzzi.html

CARLO LOVADINA: carlo.lovadina@unipv.it
Dipartimento di Matematica, Università degli Studi di Pavia, Via Ferrata 1, 27100 Pavia, Italy
http://www-dimat.unipv.it/lovadina/

JOURNAL OF MECHANICS OF MATERIALS AND STRUCTURES

http://www.jomms.org

Founded by Charles R. Steele and Marie-Louise Steele

See inside back cover or http://www.jomms.org for submission guidelines.

JoMMS (ISSN 1559-3959) is published in 10 issues a year. The subscription price for 2010 is US $500/year for the electronic version, and $660/year (+$60 shipping outside the US) for print and electronic. Subscriptions, requests for back issues, and changes of address should be sent to Mathematical Sciences Publishers, Department of Mathematics, University of California, Berkeley, CA 94720–3840.

JoMMS peer-review and production is managed by EditFLOW™ from Mathematical Sciences Publishers.

PUBLISHED BY

mathematical sciences publishers

http://www.mathscipub.org

A NON-PROFIT CORPORATION

Typeset in LaTeX

Journal of Mechanics of Materials and Structures

Volume 5, No. 5 May 2010

Axial compression of hollow elastic spheres ROBERT SHORTER, JOHN D. SMITH, VINCENT A. COVENEY and JAMES J. C. BUSFIELD 693

Coupling of peridynamic theory and the finite element method BAHATTIN KILIC and ERDOGAN MADENCI 707

Genetic programming and orthogonal least squares: a hybrid approach to modeling the compressive strength of CFRP-confined concrete cylinders AMIR HOSSEIN GANDOMI, AMIR HOSSEIN ALAVI, PARVIN ARJMANDI, ALIREZA AGHAEIFAR and REZA SEYEDNOUR 735

Application of the Kirchhoff hypothesis to bending thin plates with different moduli in tension and compression XIAO-TING HE, QIANG CHEN, JUN-YI SUN, ZHOU-LIAN ZHENG and SHAN-LIN CHEN 755

A new modeling approach for planar beams: finite-element solutions based on mixed variational derivations FERDINANDO AURICCHIO, GIUSEPPE BALDUZZI and CARLO LOVADINA 771

SIFs of rectangular tensile sheets with symmetric double edge defects XIANGQIAO YAN, BAOLIANG LIU and ZHAOHUI HU 795

A nonlinear model of thermoelastic beams with voids, with applications YING LI and CHANG-JUN CHENG 805

Dynamic stiffness vibration analysis of thick spherical shell segments with variable thickness ELIA EFRAIM and MOSHE EISENBERGER 821

Application of a matrix operator method to the thermoviscoelastic analysis of composite structures ANDREY V. PYATIGORETS, MIHAI O. MARASTEANU, LEV KHAZANOVICH and HENRYK K. STOLARSKI 837